REPORT No. 688

AERODYNAMIC CHARACTERISTICS OF HORIZONTAL TAIL SURFACES

By Abe Silverstein and S. Katzoff

SUMMARY

Collected data are presented on the aerodynamic characteristics of 17 horizontal tail surfaces including several with balanced elevators and two with end plates. Curves are given for coefficients of normal force, drag, and elevator hinge moment. A limited analysis of the results has been made. The normal-force coefficients are in better agreement with the lifting-surface theory of Prandtl and Blenk for airfoils of low aspect ratio than with the usual lifting-line theory. Only partial agreement exists between the elevator hinge-moment coefficients and those predicted by Glauert's thin-airfoil theory.

INTRODUCTION

The balance, control, and stability problems that attend the use of wing flaps on airplanes require for their solution accurate methods of predicting the forces on the horizontal tail surfaces. In order to aid in the development of such methods, the available data for 17 horizontal tail surfaces have been collected from various sources (see table I) and are herein presented. These data refer to the tail surfaces alone, exclusive of fuselage and slipstream interference. Some analyses, particularly with reference to normal-force and elevator hinge-moment coefficients, have been made within the limitations imposed by low test Reynolds Numbers and variations in section and in plan form. The data are not entirely satisfactory because the usual uncertainty exists in the extrapolation to higher Reynolds Numbers and the experimental precision is, in most cases, unknown. The results should be useful, however, until more comprehensive investigations are made.

Tables I and II contain the descriptive data for the 17 surfaces. The tails have symmetrical sections; elliptical, rectangular, and trapezoidal plan forms; aspect ratios between 3 and 4.3; and elevator areas of from 30 to 50 percent of the total tail area. Two cases of tail assemblies with twin rudders as end plates are included. In some cases, groups of tail surfaces were tested in which only one characteristic, such as the elevator balance area or the ratio of the elevator area to the tail area, was systematically varied.

SYMBOLS

A aspect ratio.

R Reynolds Number.

V velocity.

C_N normal-force coefficient ($C_L \cos \alpha_t + C_D \sin \alpha_t$).

H_e elevator hinge moment.

C_{h_e} elevator hinge-moment coefficient ($H_e/q\overline{c_e}^2\,b_e$).

α_t angle of attack of the tail, deg.

δ_e elevator angle (downward deflection positive).

S area.

b span.

c chord.

$\overline{c}$ average chord.

$\overline{c^2}$ average of chords squared.

a_0 section slope of lift curve (deg measure).

k slope of tail normal-force curve ($dC_N/d\alpha_t$).

r factor in the expression for the slope of the normal-force curve for tail surfaces with end plates.

τ elevator effectiveness.

h height of end plate.

u, v coefficients of C_N and δ_e in the hinge-moment equation.

Subscripts:

  t entire tail.

  e elevator, excluding balance.

  b balance.

NORMAL-FORCE COEFFICIENT

The tail-surface characteristic necessary for stability calculations is the rate of change of normal force with angle of attack. For control problems, the most essential characteristic is the rate of change of normal force with elevator angle. The normal-force coefficients C_N are plotted in figures 1 to 17 against angle of attack α_t, with elevator deflection δ_e as a parameter. The curves are straight and parallel over most of the useful range; nonlinearity or nonparallelism at low values of α_t is associated with large elevator deflections or protruding balances. (Cf. figs. 1 and 9.) Cross plots of C_N against δ_e for several values of α_t are shown for tail surfaces 1, 2, and 3 in figures 18 to 20. Curves of this type are of particular value in showing the variation of elevator effectiveness with elevator deflection.
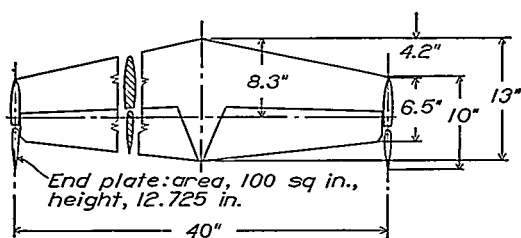
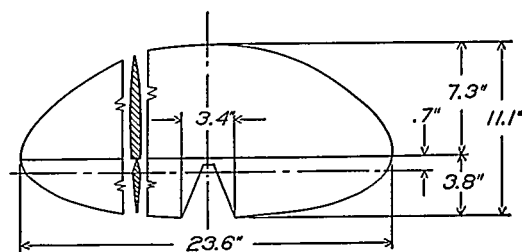## TABLE I—DIMENSIONS OF TAIL SURFACES
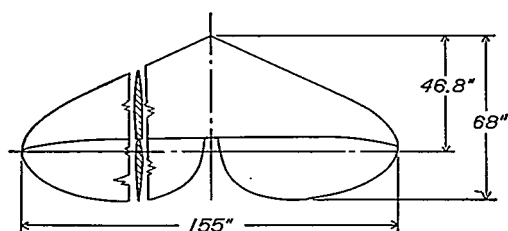
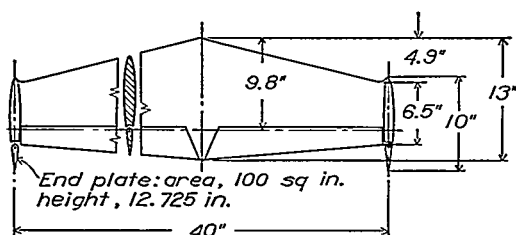Tail surface 1, unpublished data from files of full-scale wind tunnel.
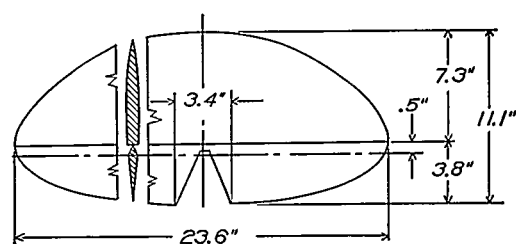
Tail surface 5, reference 1.

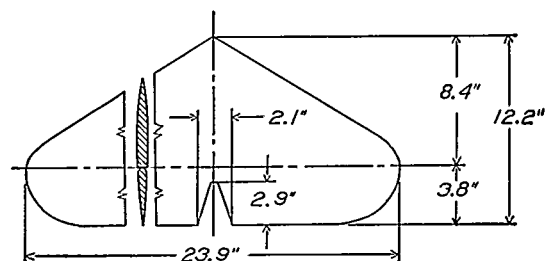End plate: area, 100 sq in., height, 12.725 in.

Tail surface 2, unpublished data from files of 7- by 10-foot wind tunnel.
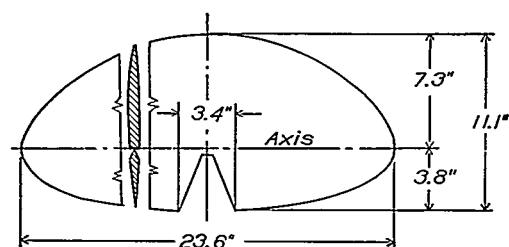
Tail surface 6, reference 1.
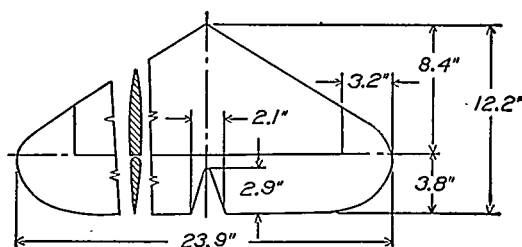
End plate: area, 100 sq in. height, 12.725 in.

Tail surface 3, unpublished data from files of 7- by 10-foot wind tunnel.
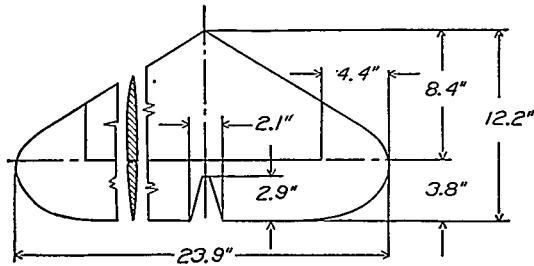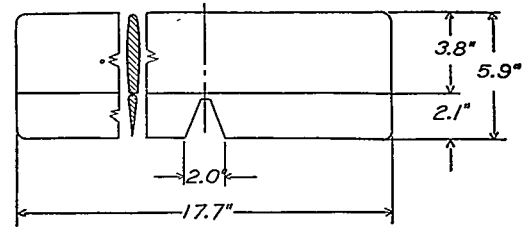
Tail surface 7, reference 1.

Tail surface 4, reference 1.
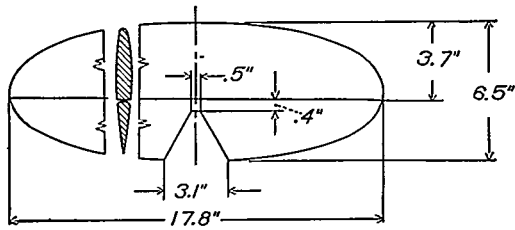
Tail surface 8, reference 1.

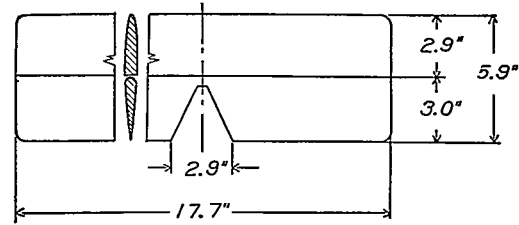| Tail surface	A	b (in.)	S_t (sq in.)	S_e (sq in.)	S_e/S_t	$\overline{c}_t$ (in.)	$\overline{c}_e$ (in.)	$\overline{c}_e/\overline{c}_t$	$\overline{c_e^2}$ (sq in.)	$\overline{c}_b$ (in.)	S_b/S_e	Test V (f p s)	Test R
1	3.4	155.0	7,015	2,450	0.35	45.25	15.80	0.35	292.0	4.31	0.27	88.0	1,960,000
2	4.1	40.0	390	131	.34	9.75	3.27	.34	11.0	.88	.25	117.3	609,000
3	4.1	40.0	390	92	.24	9.75	2.29	.24	5.6	0	0	117.3	600,000
4	3.1	23.6	181	68	.37	7.68	2.86	.37	9.0	0	0	110.0	448,000
5	3.1	23.6	181	55	.30	7.68	2.33	.30	6.2	.53	.23	110.0	448,000
6	3.0	23.6	181	51	.28	7.68	2.16	.28	5.3	.72	.33	110.0	448,000
7	3.0	23.9	192	81	.42	8.03	3.40	.42	12.0	0	0	110.0	470,000
8	3.0	23.9	192	81	.42	8.03	3.40	.42	12.0	1.85	.14	110.0	470,000

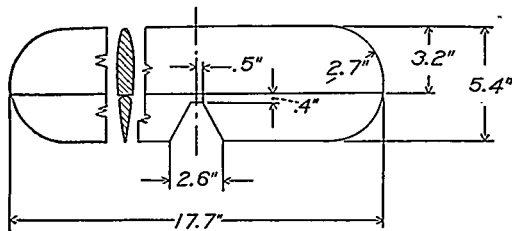Tail surface 9, reference 1.

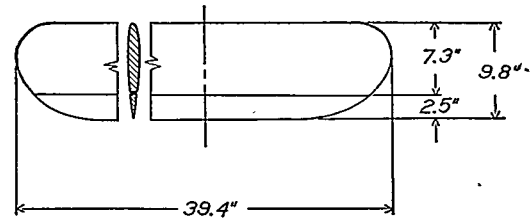Tail surface 13, reference 1.
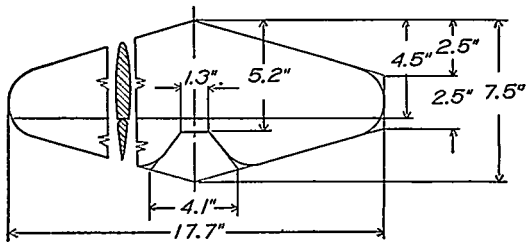

Tail surface 10, reference 2.
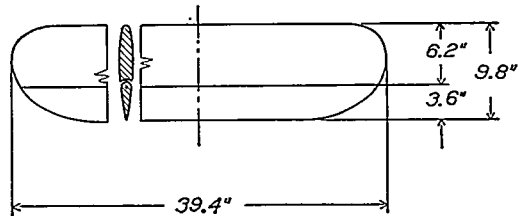

Tail surface 14, reference 1.
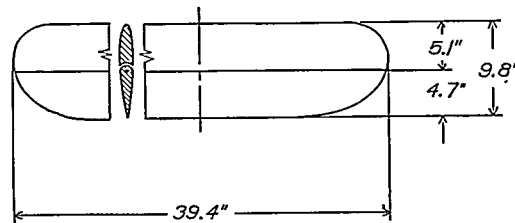

Tail surface 11, reference 2.

Tail surface 15, reference 3.

Tail surface 12, reference 2.

Tail surface 16, reference 3

Tail surface 17, reference 3.

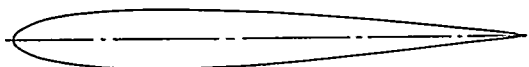| Tail surface	A	b (in.)	S_t (sq in.)	S_e (sq in.)	S_e/S_t	$\bar{c}_t$ (in.)	$\bar{c}_e$ (in.)	$\overline{c_e/c_t}$	$\overline{c_e^2}$ (sq in.)	$\bar{c}_b$ (in.)	S_b/S_e	Test V (f p s)	Test R
9	3.0	23.9	192	81	0.42	8.03	3.40	0.42	12.0	2.28	0.25	110.0	470,000
10	3.7	17.8	86	32	.37	4.84	1.82	.38	3.6	0	0	98.4	253,200
11	3.6	17.7	87	35	.40	4.88	1.97	.40	4.5	0	0	98.4	255,000
12	3.8	17.7	82	23	.28	4.62	1.32	.29	2.1	0	0	98.4	241,700
13	3.1	17.7	103	34	.33	5.83	1.94	.33	4.1	0	0	110.0	340,500
14	3.1	17.7	100	50	.50	5.67	2.84	.50	8.8	0	0	110.0	331,500
15	4.3	39.4	361	81	.23	9.15	2.27	.25	5.4	.43	.25	--------	--------
16	4.3	39.4	361	117	.32	9.15	3.12	.34	10.3	.48	.15	--------	--------
17	4.3	39.3	356	162	.45	9.06	4.20	.46	18.5	.56	.10	--------	--------

TABLE II—THICKNESSES OF TAIL-SURFACE SECTIONS   (Stations and thicknesses in percent chord)
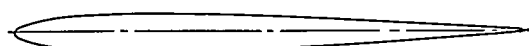
Sta.	Thick.	Sta.	Thick.	Sta.	Thick.
0	0	30	7.73	70	4.66
5	4.66	40	7.26	80	3.47
10	6.26	50	6.53	90	1.93
20	7.53	60	5.73	100	.11

Tail surface 1.

Sta.	Thick.	Sta.	Thick.	Sta.	Thick.
0	0	30	12.70	70	8.40
5	6.90	40	12.70	80	6.00
10	9.40	50	11.70	90	3.00
20	11.70	60	10.30	100	.00

Tail surfaces 10, 11, 12, 15, 16, and 17—Göttingen 409.

Sta.	Thick.	Sta.	Thick.	Sta.	Thick.
0	0	30	12.00	70	7.32
5	7.12	40	11.60	80	5.24
10	9.36	50	10.58	90	2.90
20	11.48	60	9.12	100	.24

Tail surfaces 2 and 3—N. A. C. A. 0012.

Sta.	Thick.	Sta.	Thick.	Sta.	Thick.
0	0	30	8.62	70	6.19
5	4.27	40	8.75	80	4.63
10	5.94	50	8.34	90	2.68
20	7.80	60	7.52	100	.30

Tail surfaces 7, 8, and 9.

Sta.	Thick.	Sta.	Thick.	Sta.	Thick.
0	0	30	7.74	70	4.84
5	3.01	40	7.74	80	3.30
10	4.76	50	7.06	90	1.79
20	6.92	60	6.10	100	.30

Tail surfaces 4, 5, and 6.

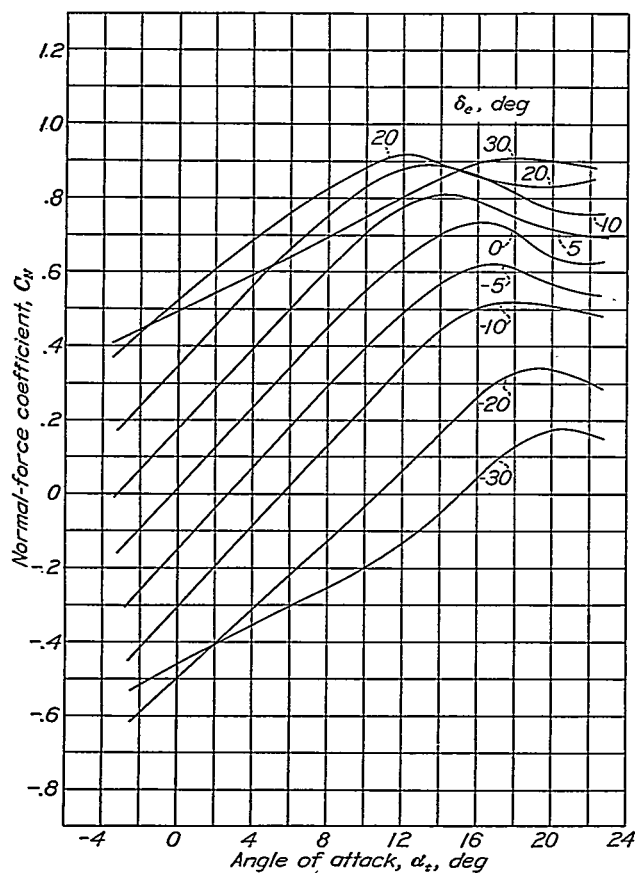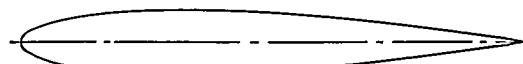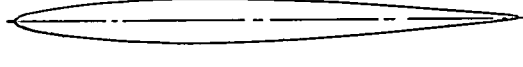| Sta.	Thick.	Sta.	Thick.	Sta.	Thick.
0	0	30	8.08	70	5.42
5	4.68	40	8.00	80	3.98
10	6.10	50	7.48	90	2.30
20	7.56	60	6.60	100	.40

Tail surfaces 13 and 14.

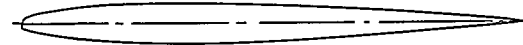FIGURE 1.—Normal-force coefficient against angle of attack at various elevator deflections for tail surface 1.
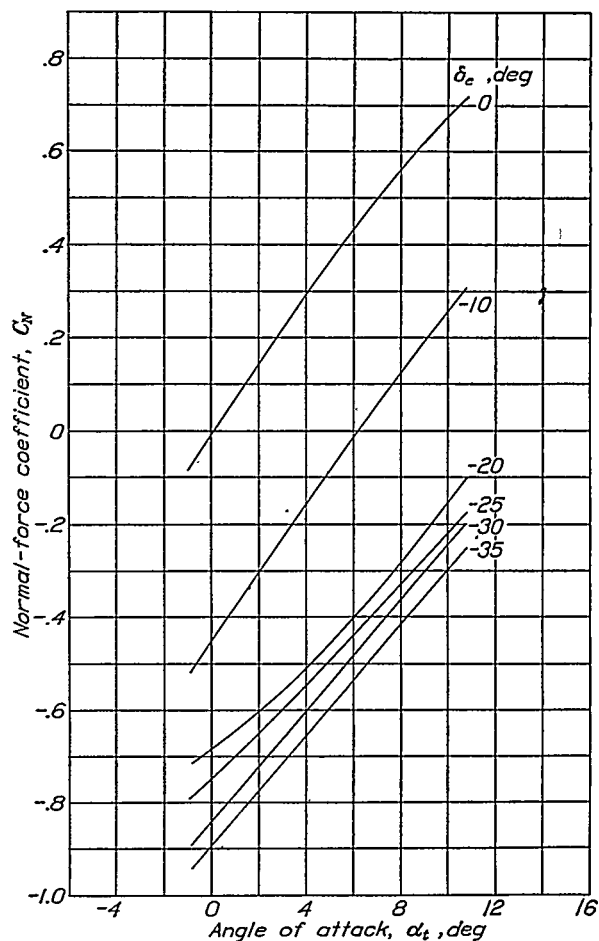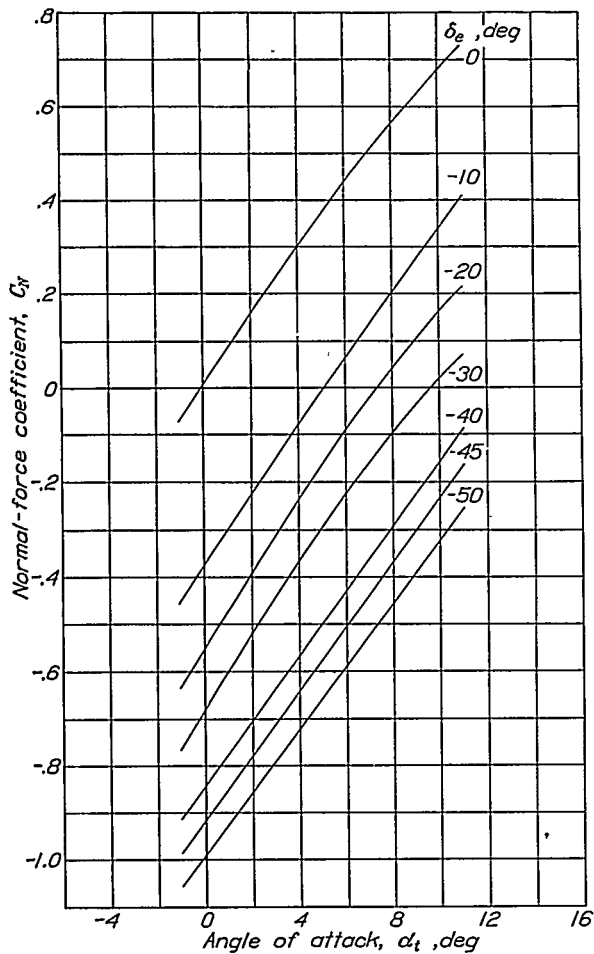

FIGURE 2.—Normal-force coefficient against angle of attack at various elevator deflections for tail surface 2.

FIGURE 3.—Normal-force coefficient against angle of attack at various elevator deflections for tail surface 3.
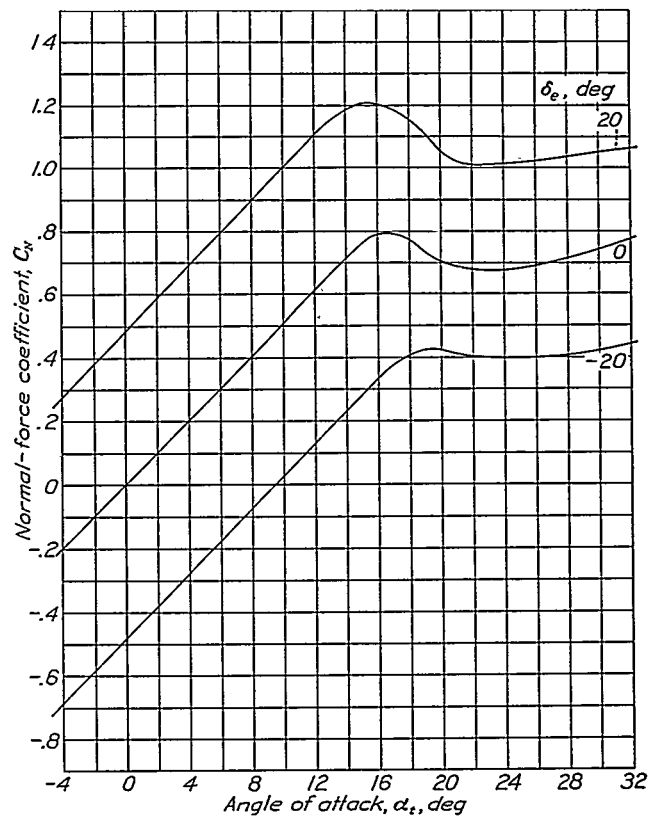

FIGURE 4.—Normal-force coefficient against angle of attack at various elevator deflections for tail surface 4.
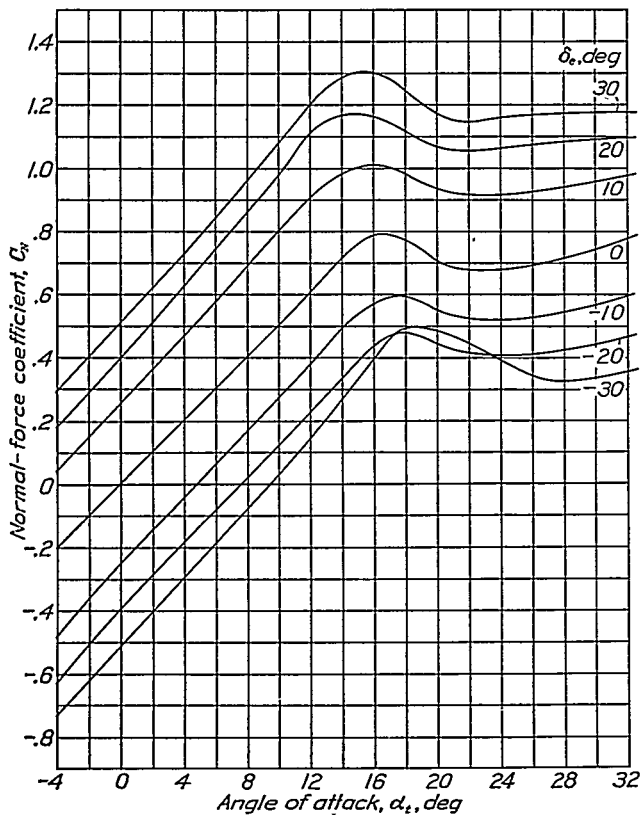

FIGURE 5.—Normal-force coefficient against angle of attack at various elevator deflections for tail surface 5.
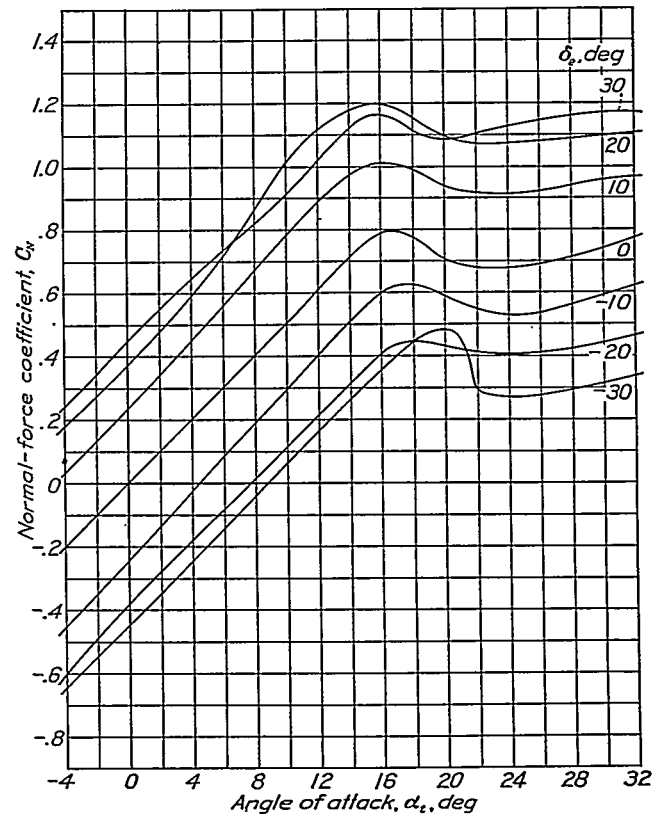

FIGURE 6.—Normal-force coefficient against angle of attack at various elevator deflections for tail surface 6.
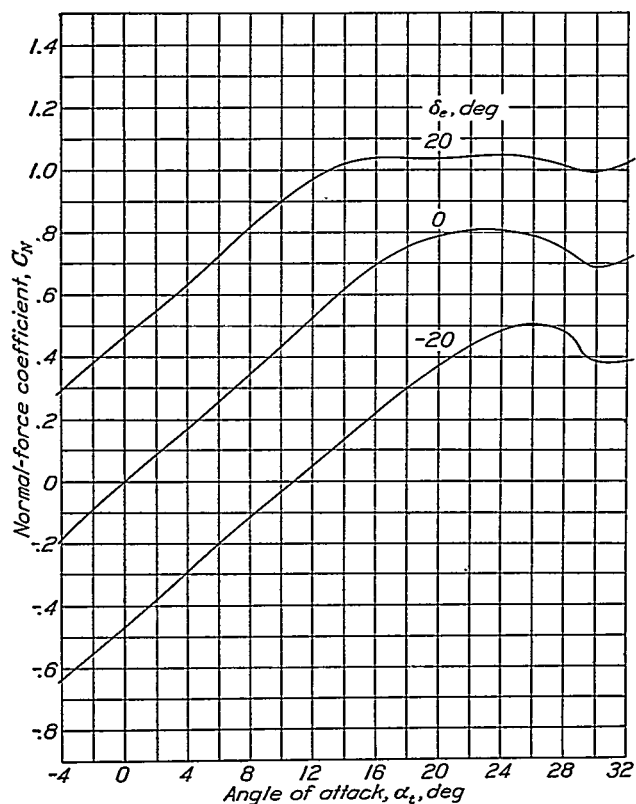
FIGURE 7.—Normal-force coefficient against angle of attack at various elevator deflections for tail surface 7.

FIGURE 9.—Normal-force coefficient against angle of attack at various elevator deflections for tail surface 9.

FIGURE 8.—Normal-force coefficient against angle of attack at various elevator deflections for tail surface 8.

FIGURE 10.—Normal-force coefficient against angle of attack at various elevator deflections for tail surface 10.

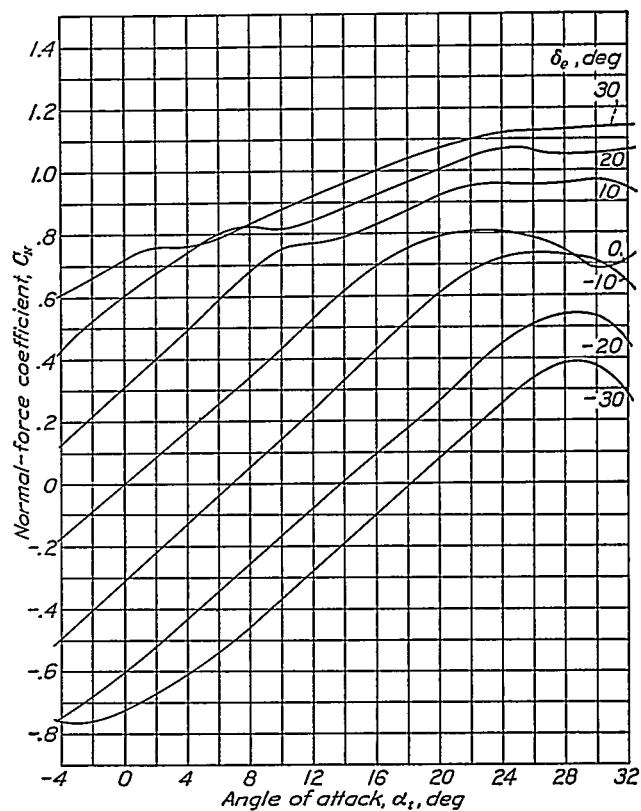FIGURE 11.—Normal-force coefficient against angle of attack at various elevator deflections for tail surface 11.

FIGURE 13.—Normal-force coefficient against angle of attack at various elevator deflections for tail surface 13.
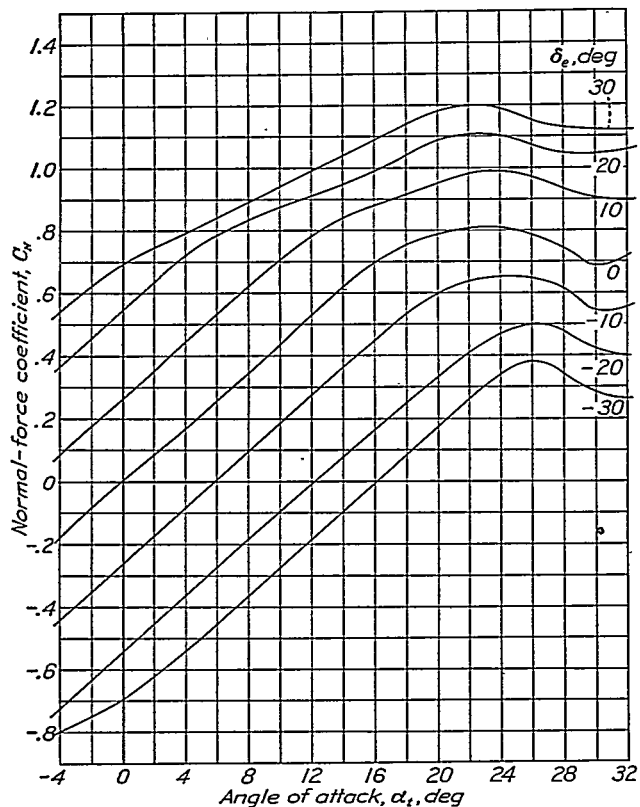
FIGURE 12.—Normal-force coefficient against angle of attack at various elevator deflections for tail surface 12.
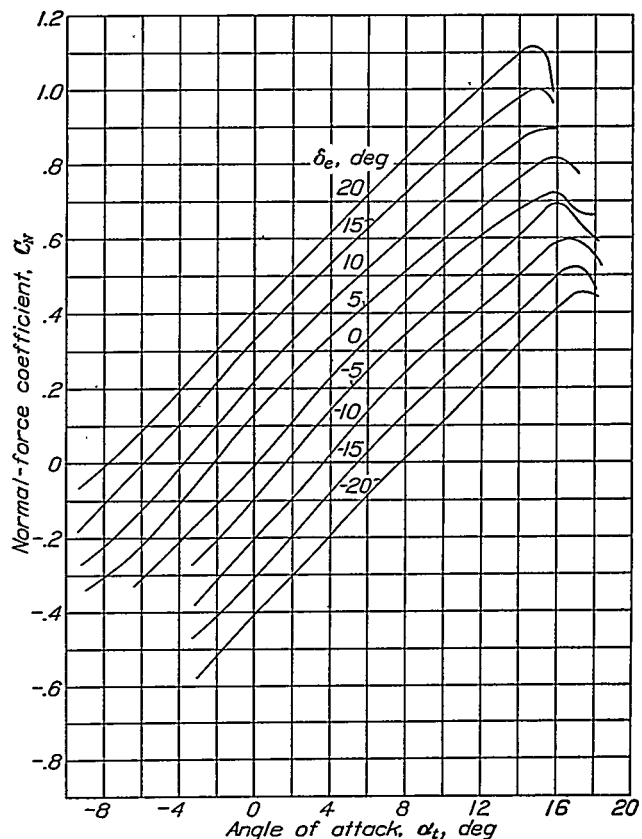
FIGURE 14.—Normal-force coefficient against angle of attack at various elevator deflections for tail surface 14.
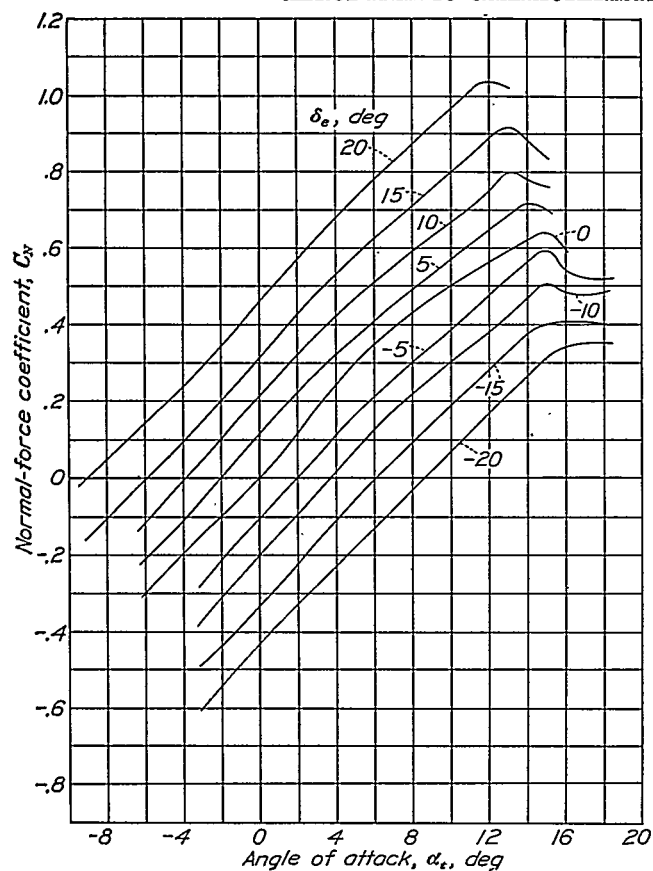
FIGURE 15.—Normal-force coefficient against angle of attack at various elevator deflections for tail surface 15.
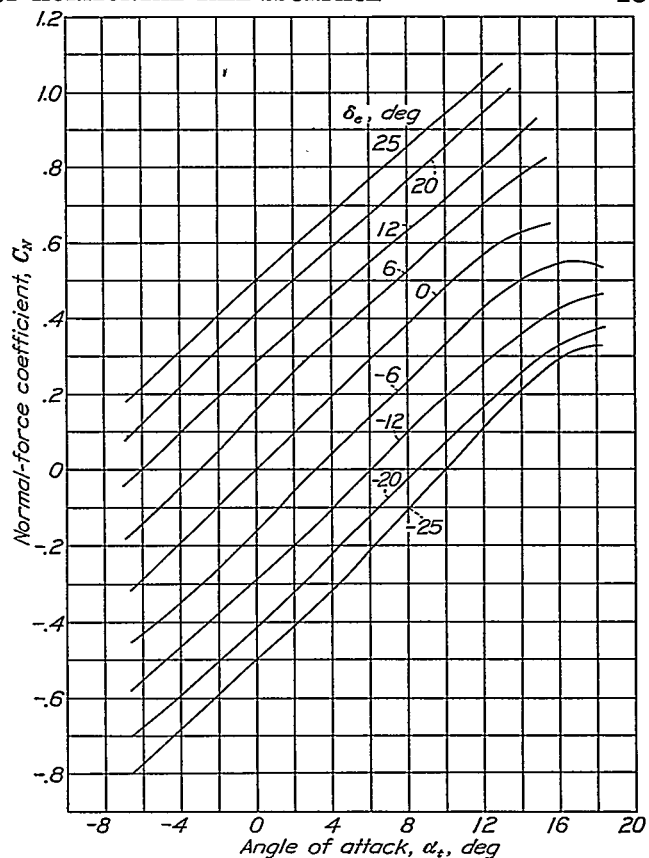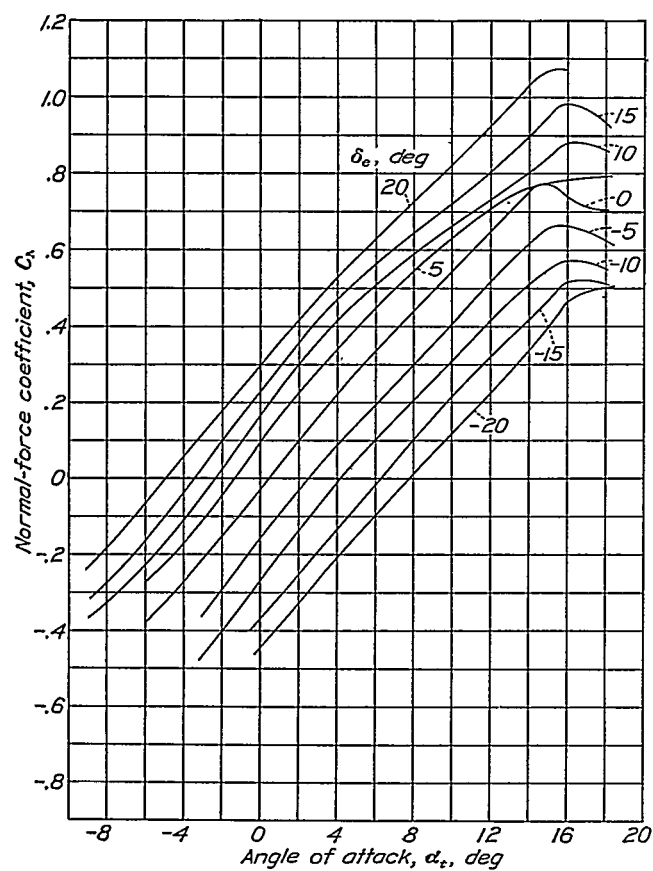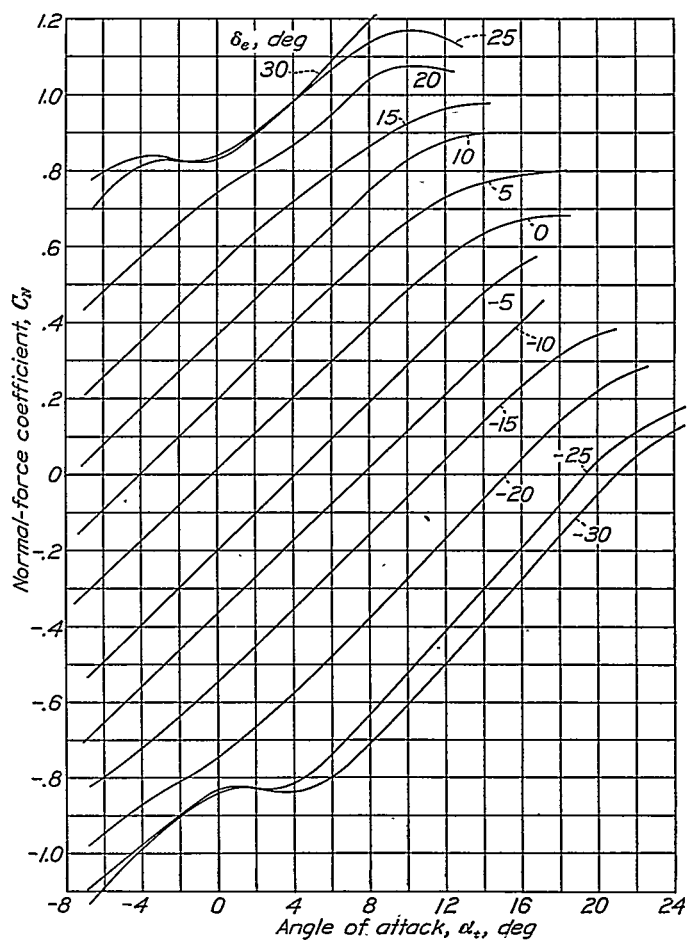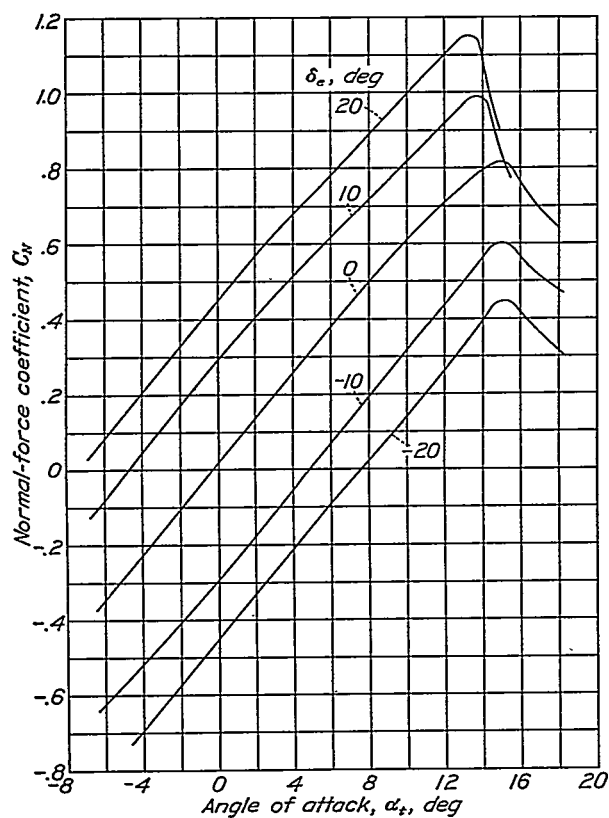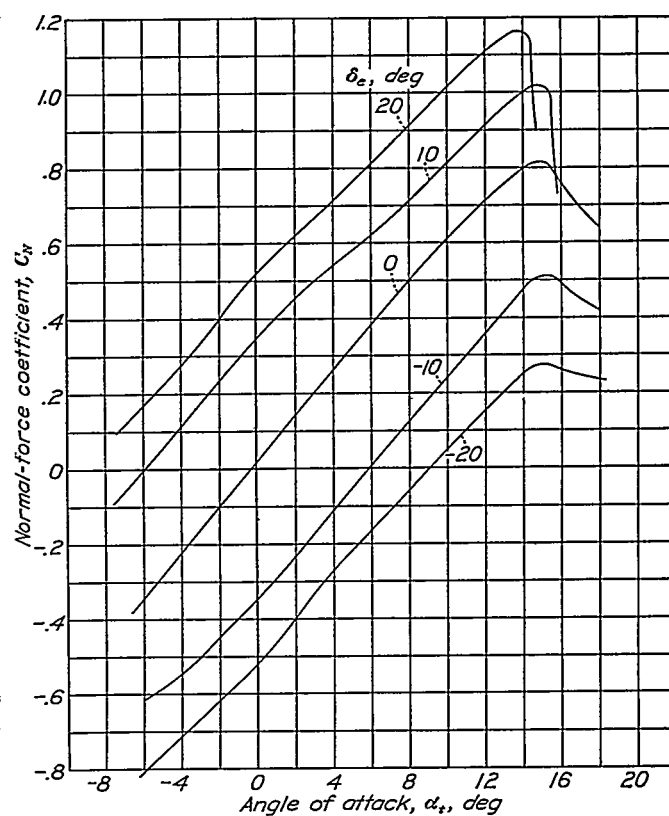
FIGURE 16.—Normal-force coefficient against angle of attack at various elevator deflections for tail surface 16.
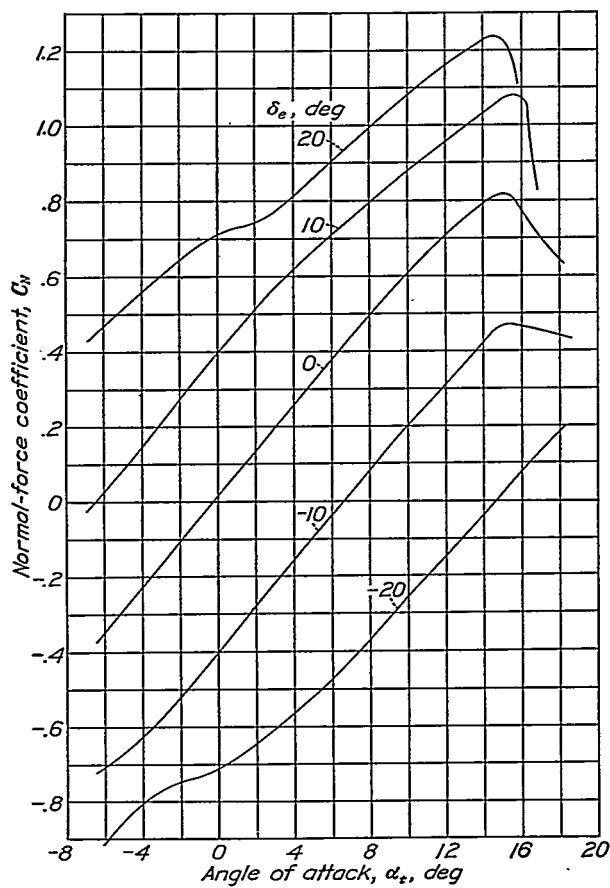

FIGURE 17.—Normal-force coefficient against angle of attack at various elevator deflections for tail surface 17.

Some correlation between experimental results and theory has been attempted. The normal force can be expressed (reference 4) in the form

$$C_N = k(\alpha_t + \tau\delta_e) \qquad (1)$$

The value of k, or $dC_N/d\alpha_t$, depends mainly on the aspect ratio. According to lifting-line theory, this

gations (references 6 and 7) for wings and plates of low aspect ratio with rounded tips. The observed reductions in slope, however, somewhat exceed these predictions, probably because of the effects of the cut-outs, generally built to accommodate the rudder, and of the gaps between stabilizer and elevator.

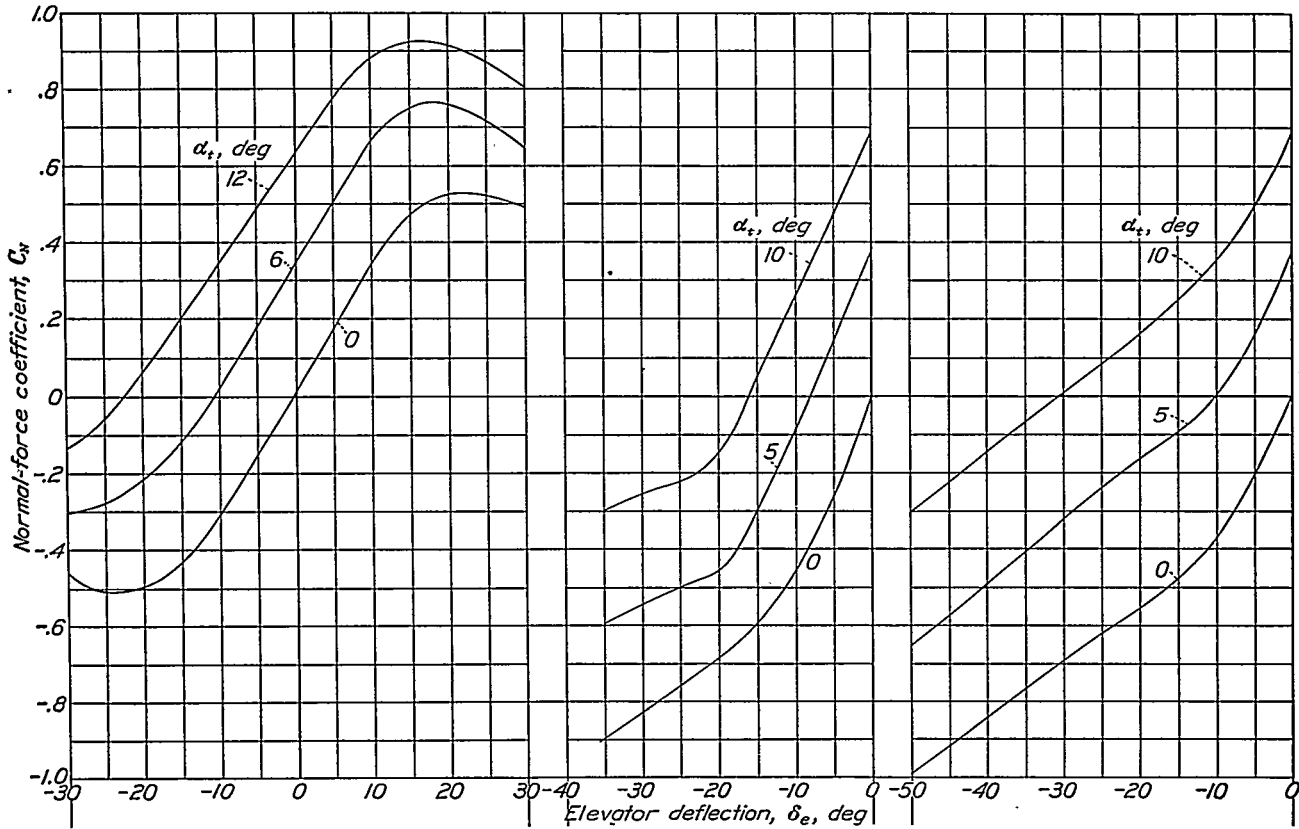The effect of the cut-out is strikingly shown by the

FIGURE 18.—Normal-force coefficient against elevator deflection at various angles of attack for tail surface 1.

FIGURE 19.—Normal-force coefficient against elevator deflection at various angles of attack for tail surface 2.

FIGURE 20.—Normal-force coefficient against elevator deflection at various angles of attack for tail surface 3.

slope should be approximately $a_0 \big/ \left(1 + \dfrac{57.3 a_0}{\pi A}\right)$. Figure 21 shows, however, that the slope decreases much more rapidly with aspect ratio than does the value of this expression. Such behavior has been predicted by Prandtl and by Blenk (reference 5) from theoretical considerations and has been observed in other investi-

407300°—41——13

comparisons in figures 22 and 23. In both cases, the slope of the lift curve was reduced about 2 percent by the cut-out; whereas, if aspect ratio were the sole determining factor, the slope would have been increased by about 4 percent. The net reduction in $dC_{N_t}/d\alpha_t$, due to the cut-outs, was thus about 6 percent in these cases.

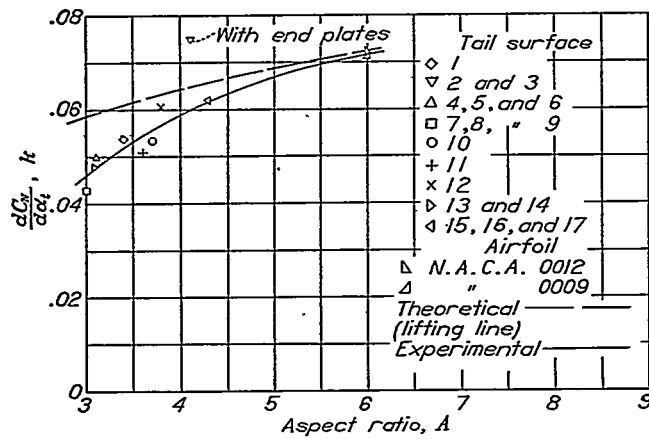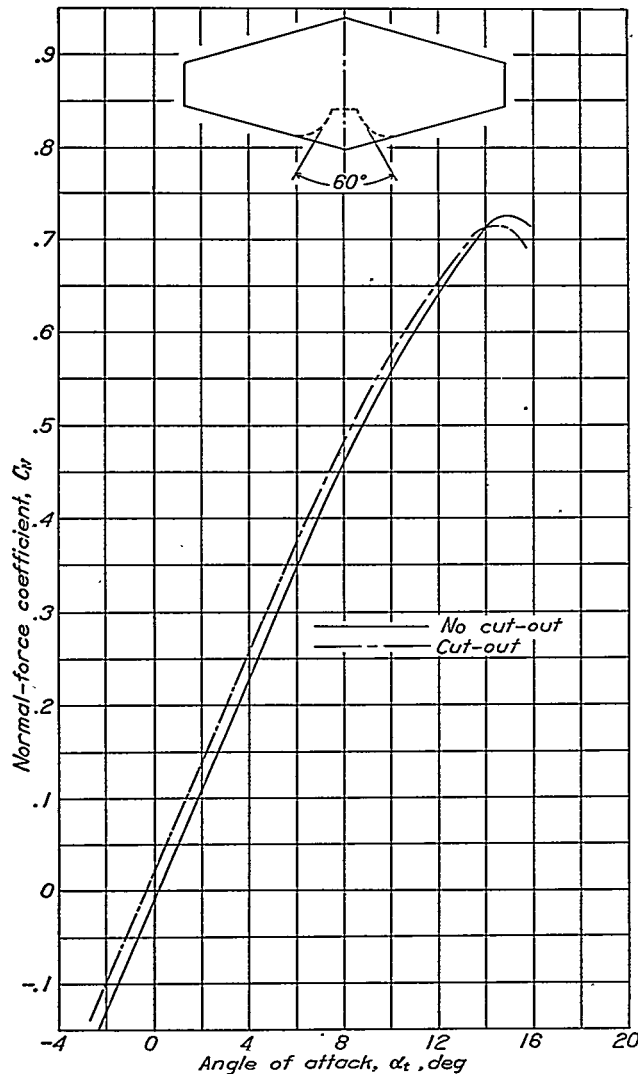FIGURE 21.—Variation of the parameter k with aspect ratio and comparison with theory.

FIGURE 22.—Effect of a cut-out on the normal-force coefficient of a Göttingen 409 airfoil (reference 2).
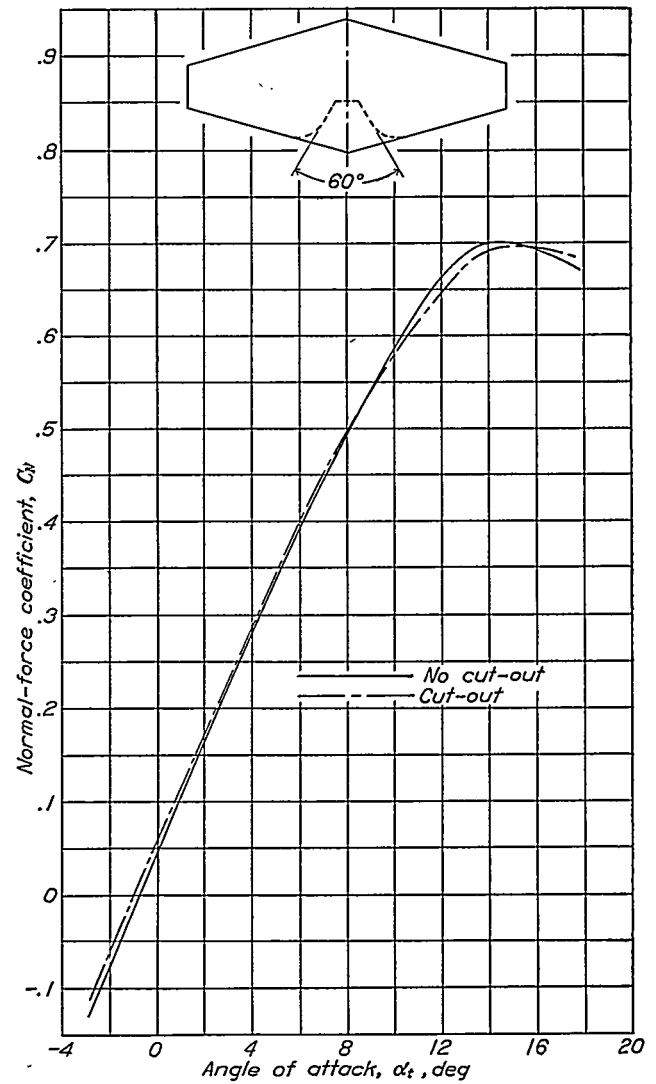

FIGURE 23.—Effect of a cut-out on the normal-force coefficient on a Göttingen 177 airfoil (reference 2).
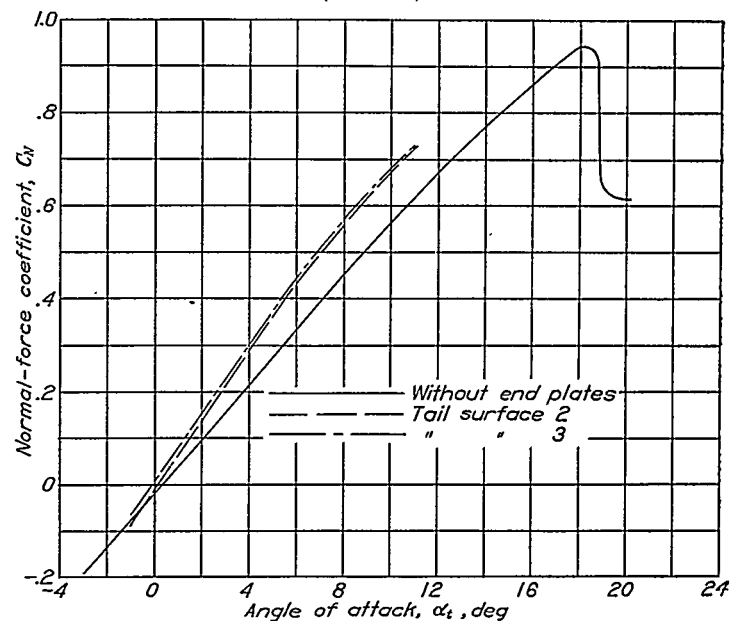

FIGURE 24.—Effect of end plates on the slope of the normal-force curve of tail surfaces 2 and 3.

A gap between the stabilizer and the elevator is, in general, detrimental although the published data on the subject are either merely qualitative or incomplete (references 8 and 9). Seiferth (reference 3) states that, in preliminary tests, the gap was found to have a negligible effect; the gap tested was narrow and of the most favorable type, being between a rounded concave trailing edge on the stabilizer and a rounded convex leading edge on the elevator. In the work on flaps reported in reference 8, the effect of the gap was easily measurable. The gap tested was a $0.0032c$ space between a flat trailing edge on the airfoil and a rounded leading edge on the flap. In the flight experiments reported in reference 9, sealing the gap greatly improved the maneuverability and the landing characteristics of the airplane; the gap, however, was of unusually poor design, consisting of a $0.02c$ gap between a rounded convex trailing edge on the stabilizer and a rounded convex leading edge on the elevator.

The normal-force curves for tail surfaces 2 and 3 with and without end plates are shown in figure 24. For the two twin-rudder tails (figs. 2 and 3), the value of $dC_N/d\alpha_t$ is about 0.074, which is considerably higher than that for any of the other tail planes. According to the theory of wings with end plates (reference 10),

$$\frac{dC_N}{d\alpha_t} = \frac{a_0}{1 + \frac{ra_0 \times 57.3}{\pi A}} \qquad (2)$$

in which r is a factor given by the curve of figure 25 as a function of h/b_t, the ratio of the height of the end plate to the tail span. For tails 2 and 3, $h/b_t = 0.32$ so that, from figure 25, $r = 0.63$. Considering $a_0 = 0.093$, it follows from equation (2) that $dC_N/d\alpha_t = 0.074$, which is in agreement with the experimental value.

The parameter τ (equation (1)) is the ratio of the effectiveness of a change in elevator angle δ_e to that of a change in tail angle α_t. It is a function mainly of the ratio of the elevator area to the total tail area S_e/S_t; however, it also depends to some extent on the relative balance area S_b/S_e, the nature of the gap, and the plan form. The experimental values of τ for the 17 tail surfaces are plotted against S_e/S_t in figure 26. Three different curves have been drawn through the points for three different values of S_b/S_e. These curves apply to tail surfaces in which the gap between the elevator and the stabilizer is open. It appears that sealing the gap may increase the value of τ by about 10 percent. For comparison, the theoretical curve (reference 4) is given.

The maximum normal force of the horizontal tail surfaces is of particular interest for airplanes characterized by early center-section stalls or large ground effects on the downwash. For these cases, the flow may break away on the upper surface of the stabilizer when the elevator is deflected upward. Stalling on the lower surface of the stabilizer, with the elevator de-
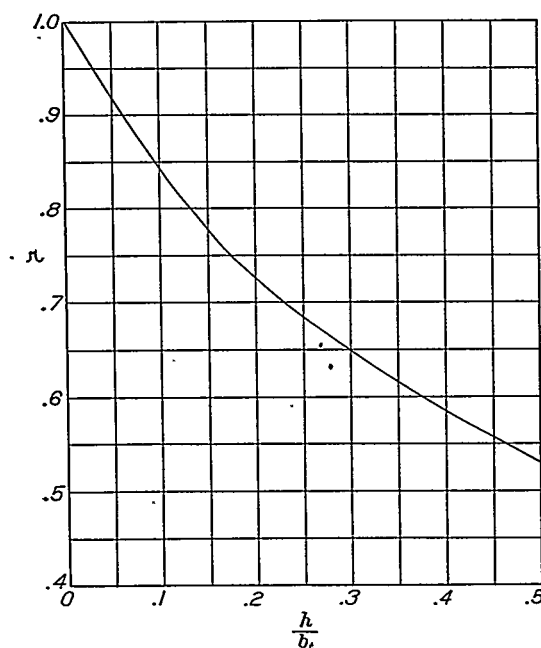

FIGURE 25.—Variation of the parameter r with the ratio of the height of the end plate to the tail span.

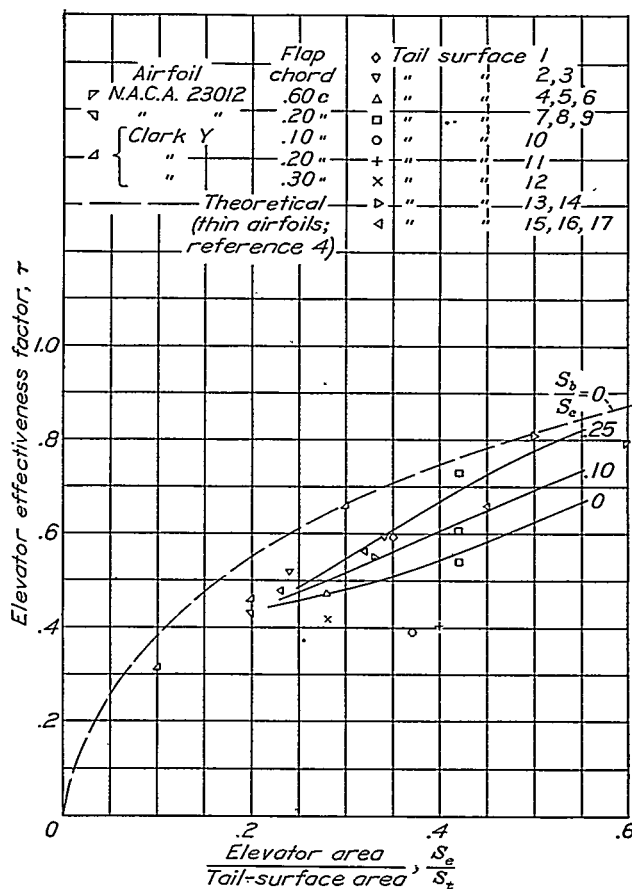$$\frac{dC_N}{d\alpha_t} = \frac{a_0}{1 + \frac{ra_0 \times 57.3}{\pi A}}$$

FIGURE 26.—Values of the parameter τ for various ratios of elevator area to tail surface area.

flected upward, may possibly occur when the airplane is near the maximum permissible speed with partial-
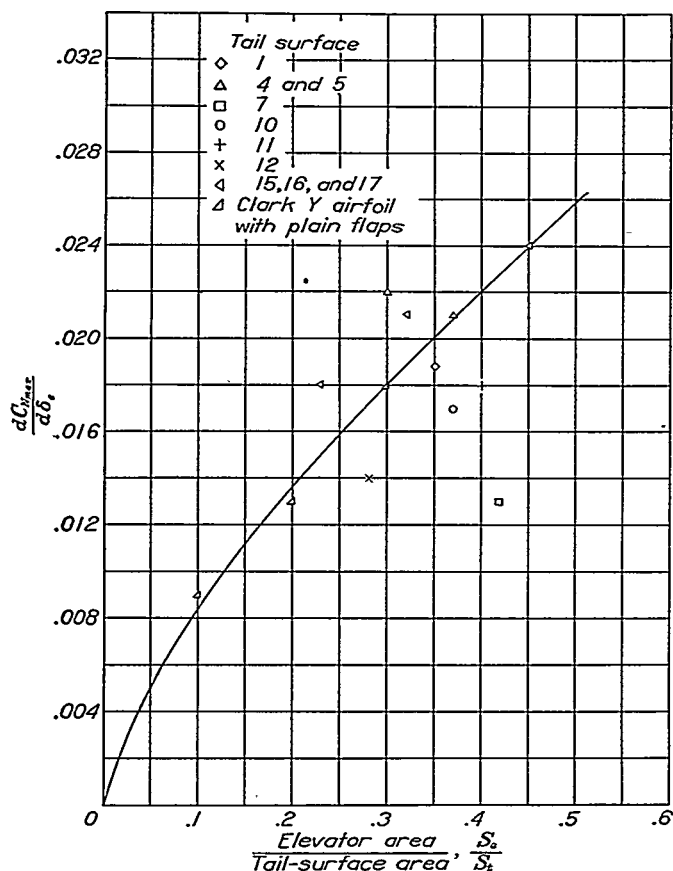

FIGURE 27.—Variation of $dC_{N_{max}}/d\delta_e$ with the ratio of elevator area to tail-surface area.
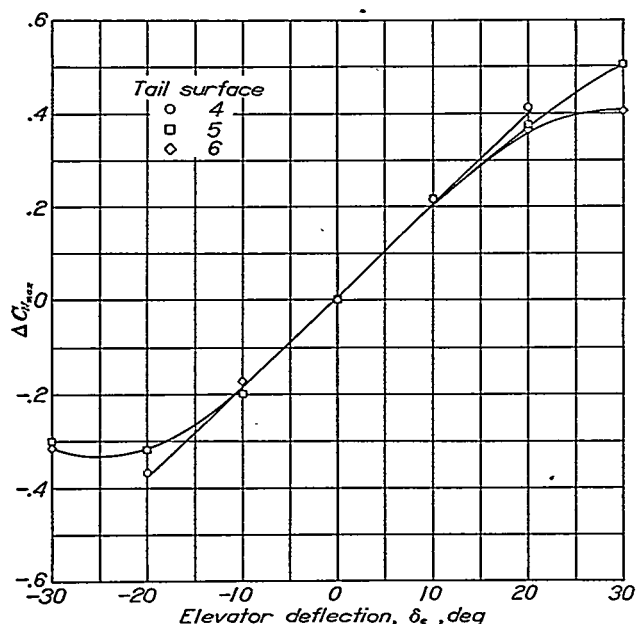

FIGURE 28.—Increment of maximum normal-force coefficient against elevator deflection for tails with offset-hinge balance.

span flaps fully deflected. This particular flight condition may occur when an airplane is waved off during

an attempted landing on an aircraft carrier or takes off immediately after landing with flaps down. It is most desirable that the elevator effectiveness be maintained at the stall. Values of $dC_{N_{max}}/d\delta_e$, taken between elevator deflections of 10° and —10°, are plotted against S_e/S_t in figure 27, together with similar data for
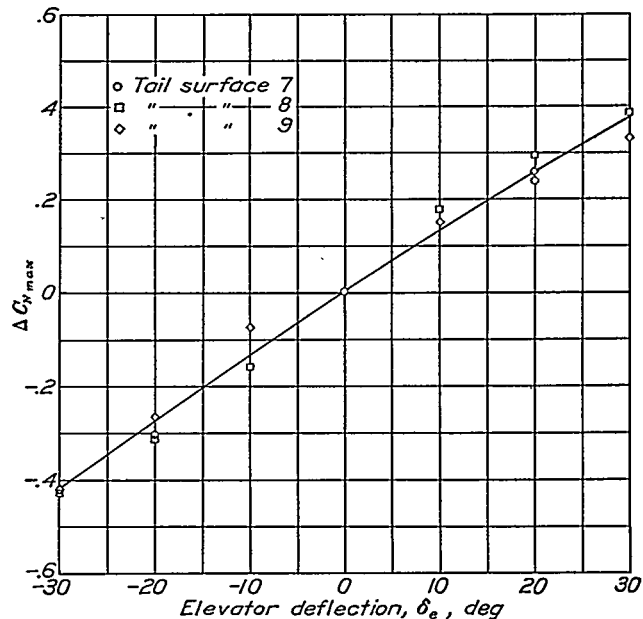

FIGURE 29.—Increment of maximum normal-force coefficient against elevator deflection for tails with overhung balance.

plain flaps on the Clark Y airfoil. The values of the maximum normal-force coefficients are given for most of the tail surfaces in figures 1 to 17.

The considerable scatter of the points in figure 27 may be attributed to the many factors upon which the maximum force depends. One important variable is probably the section thickness; thus, in the analogous
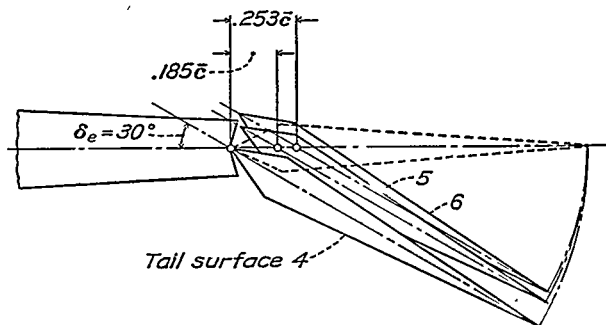
FIGURE 30.—Diagram showing elevator in deflected position on tail surfaces 4, 5, and 6.

case of flapped airfoils, the flap effectiveness has been shown (reference 8) to increase with thickness.

The gap between the elevator and the stabilizer is also an important variable. Results obtained with flapped wings showed that the increment of maximum lift due to deflecting 0.20c flaps is reduced 20 to 30 percent by a gap of only 0.003c between a convex leading edge on the flap and a flat trailing edge on the airfoil (reference 8).

Comparison of the results for tail surfaces 4, 5, and 6 (fig. 28) and for tail surfaces 7, 8, and 9 (fig. 29) shows the effect of elevator balance on the elevator effectiveness at maximum normal force. For the largest offset-hinge balance (fig. 28), the elevator effectiveness begins to decrease after about 10° deflection, and increasing the deflection beyond 20° has little effect. The discontinuity in the surface caused by the protrusion of the balance (shown in fig. 30) probably induces the stall in this case. For the overhang, or horn, type of balance (fig. 29), the effectiveness of the elevator is maintained up to 30° deflection. The rate of increase of the maximum normal force with elevator deflection is lower, however, than for the offset-hinge balance.

The range of Reynolds Numbers over which the data for elevator effectiveness are valid is unknown. Flap tests made in the N. A. C. A. 7- by 10-foot and variable-density wind tunnels (references 8 and 11) indicate, however, that the increment of maximum lift due to flap deflection is not greatly affected by the Reynolds Number.

ELEVATOR HINGE MOMENTS

The hinge-moment coefficients are plotted against elevator deflection in figures 31 to 46 for different values of angle of attack of the tail surface. No hinge moments were measured for tail surface 1. The curves are smoothest, in general, for unstalled conditions and for elevators without balances. Increasing either α_t or δ_e into the stalled range is generally accompanied by a marked variation, usually a sharp increase, in the hinge moment.

The theoretical hinge-moment coefficients for thin airfoils are derived in reference 4 for elevators without balance. They are expressed in the form

$$C_{h_e} = uC_N + v\delta_e \tag{3}$$

and theoretical curves are given for u and v as functions of the ratio c_e/c_t. The theoretical values of u derived from thin-airfoil theory, however, are somewhat higher than the theoretical values corresponding to airfoils of finite thickness. Thus, hinge-moment calculations for $c_e/c_t = 0.3$, based on the theoretical pressure distribu-

tions for the N. A. C. A. 0006 and N. A. C. A. 0018 airfoil sections, gave values for u about 0.89 and 0.73, respectively, of those given by thin-airfoil theory.

In the present analysis, experimental values for u and v were found from the curves of figures 31 to 46. Thus

$$u = \left(\frac{\partial C_{h_e}}{\partial C_N}\right)_{\delta_e}$$

$$v = \left(\frac{\partial C_{h_e}}{\partial \delta_e}\right)_{\alpha_t} - u\left(\frac{\partial C_N}{\partial \delta_e}\right)_{\alpha_t}$$

These experimental values, for tail surfaces without balanced elevators, are plotted against S_e/S_t in figures 47 and 48, which also show the theoretical curves from reference 4. The x values of u fall considerably below the theoretical curve but the x values of v are in fair agreement with the theory. The gap between the elevator and the stabilizer as well as the nonuniform distribution of c_e/c_t across the span of the tail doubtless contributes to the scatter of the points on figures 47 and 48.

Reduction of hinge moments by shifting the hinge back along the elevator (offset-hinge balance) is illustrated by tail surfaces 4, 5, and 6 (fig. 49). The effectiveness of the overhang type of balance in reducing hinge moments is shown in figures 37 and 38.

The flight experiments of reference 9 showed that, by closing the gap between the elevator and the stabilizer, the tail effectiveness was increased and the stick forces were much reduced. The gap in the case tested, however, was unusually wide.

DRAG

Several plots of drag coefficient C_D against α_t are given in figures 50 to 54. They exhibit the usual parabolic increase with angle of attack and the sharp rise after the angle of stall; however, the increase in all cases considerably exceeds that corresponding to the usual induced-drag equation, $C_{D_i} = \dfrac{C_L^2}{\pi A}$. This larger drag is attributed to the large tip losses of the surfaces of low aspect ratio.
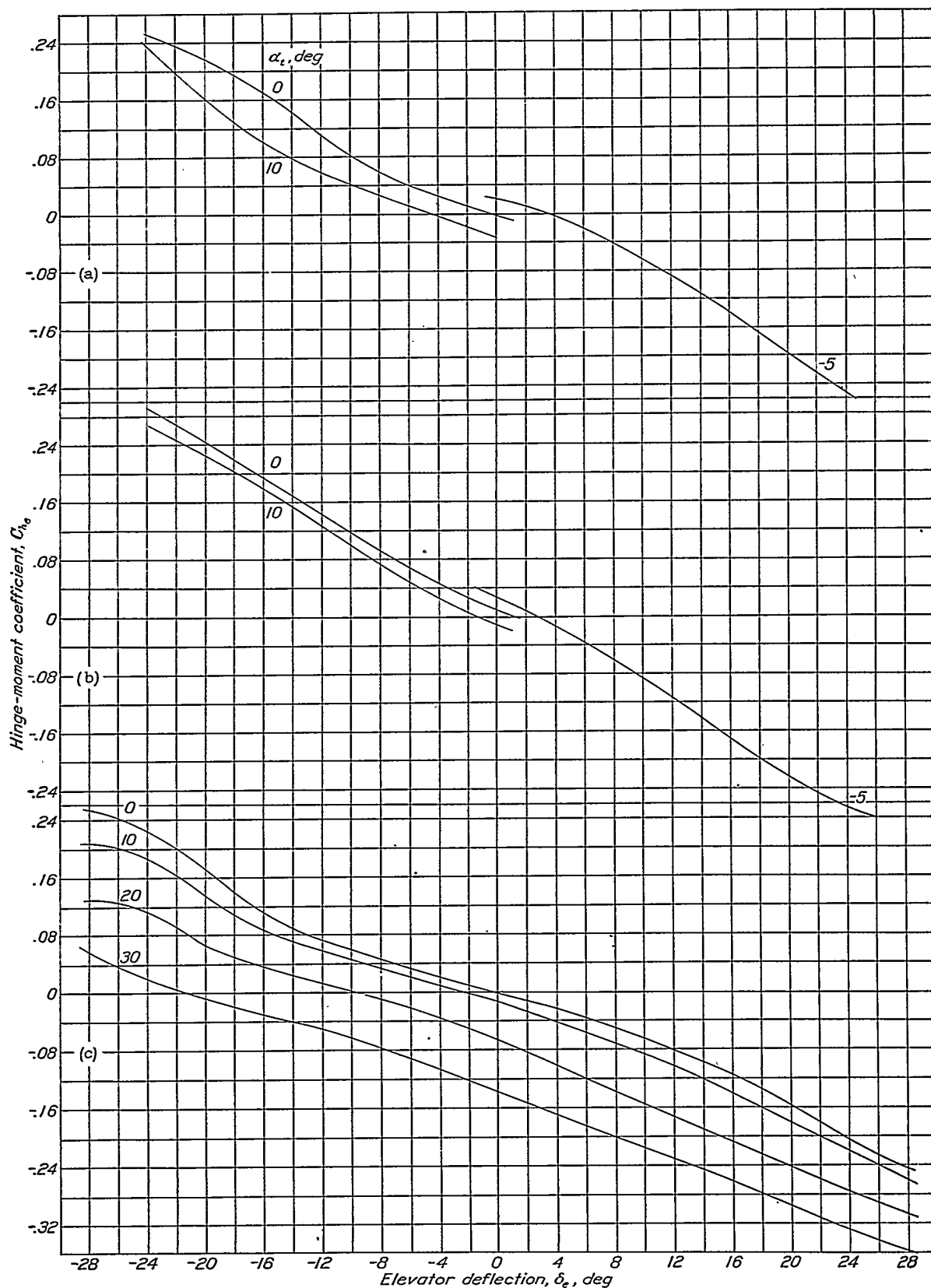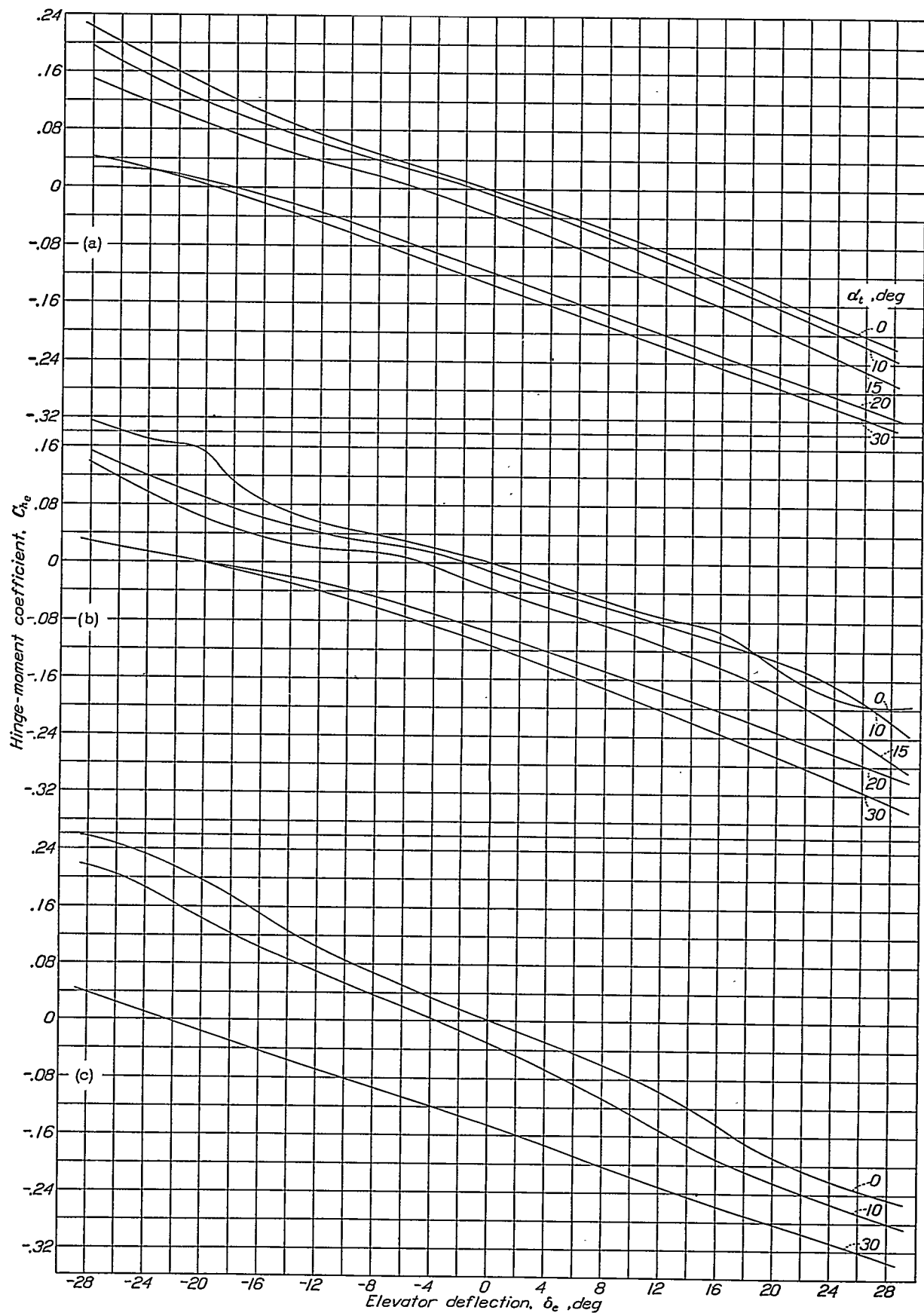
(a) Figure 31.—Tail sur-
face 2.

(b) Figure 32.—Tail sur-
face 3.

(c) Figure 33.—Tail sur-
face 4.

Elevator hinge-moment coefficient against elevator deflection at various angles of attack for tail surfaces 2, 3, and 4.
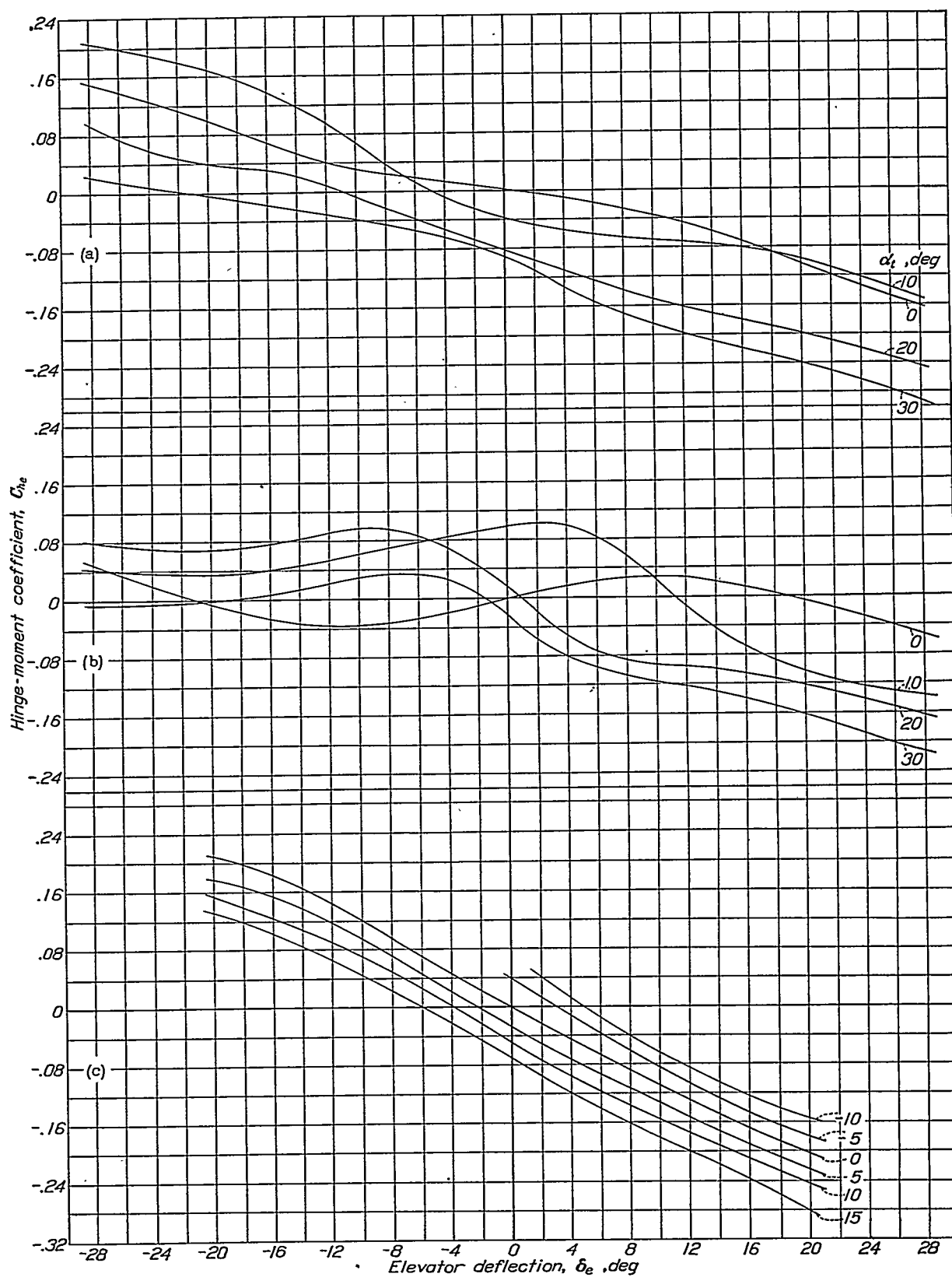
(a) FIGURE 34.—Tail surface 5.

(b) FIGURE 35.—Tail surface 6.

(c) FIGURE 36.—Tail surface 7.

Elevator hinge-moment coefficient against elevator deflection at various angles of attack for tail surfaces 5, 6, and 7.
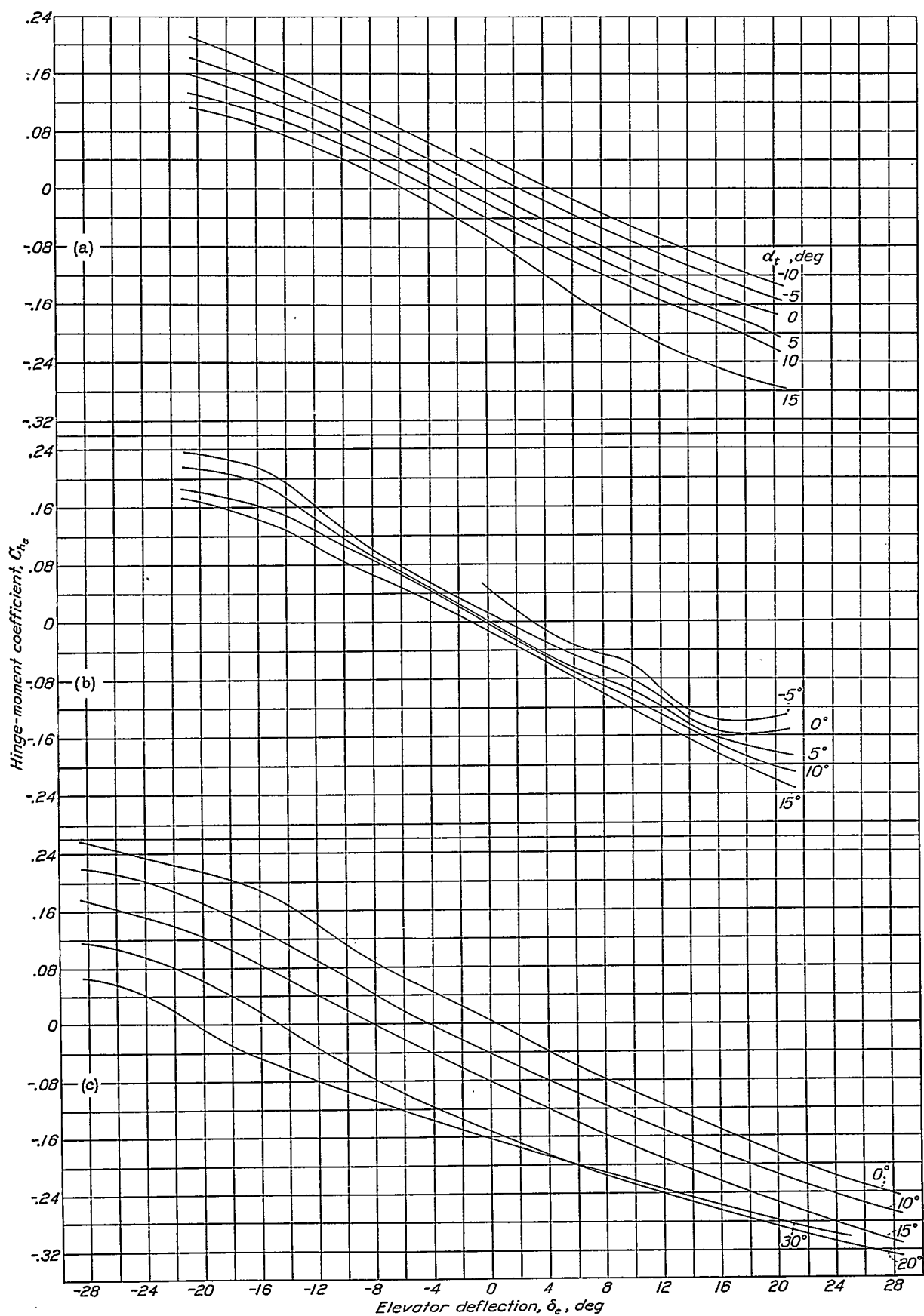
(a) FIGURE 37.—Tail surface 8.

(b) FIGURE 38.—Tail surface 9.

(c) FIGURE 39.—Tail surface 10.

Elevator hinge-moment coefficient against elevator deflection at various angles of attack for tail surfaces 8, 9, and 10.
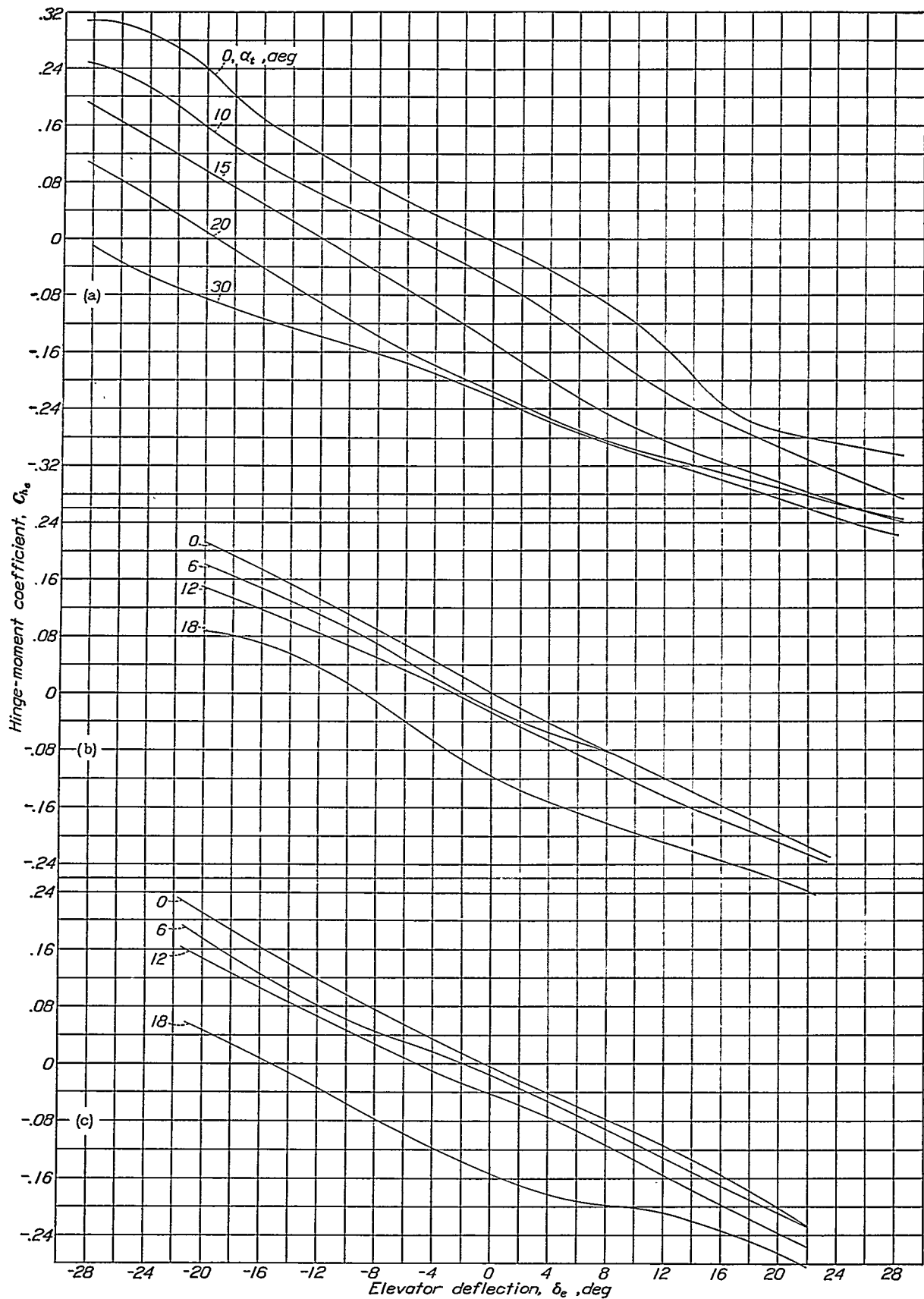
(a) FIGURE 40.—Tail surface 11.

(b) FIGURE 41.—Tail surface 12.

(c) FIGURE 42.—Tail surface 13.

Elevator hinge-moment coefficient against elevator deflection at various angles of attack for tail surfaces 11, 12, and 13.

(a) FIGURE 43.—Tail sur-
face 14.

(b) FIGURE 44.—Tail sur-
face 15.

(c) FIGURE 45.—Tail sur-
face 16.

Elevator hinge-moment coefficient against elevator deflection at various angles of attack for tail surfaces 14, 15, and 16.
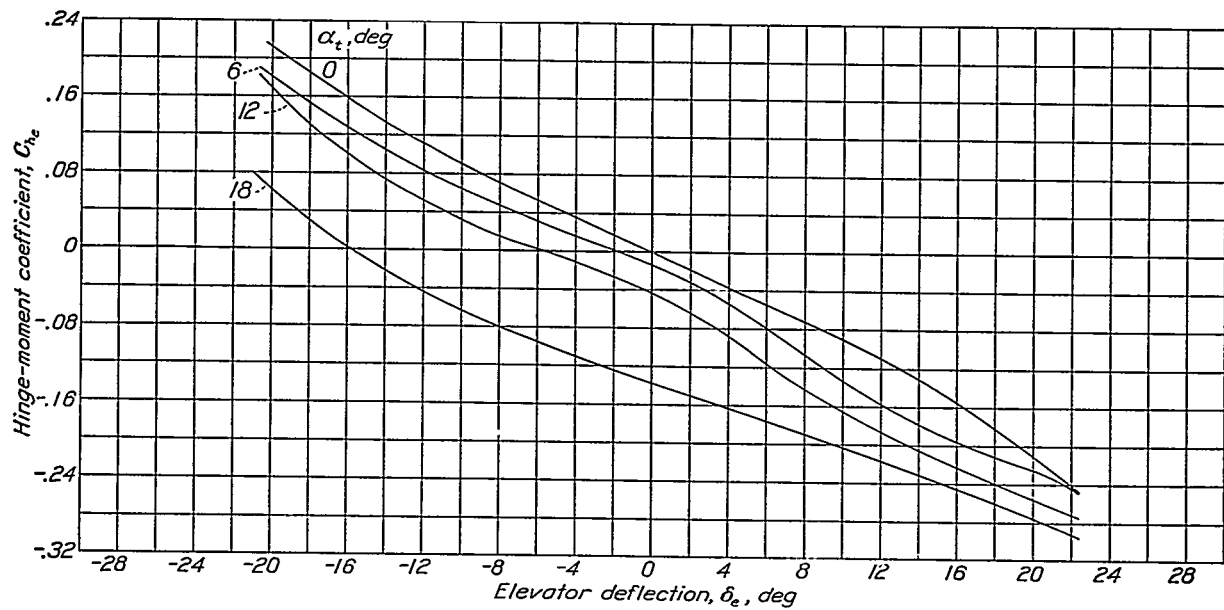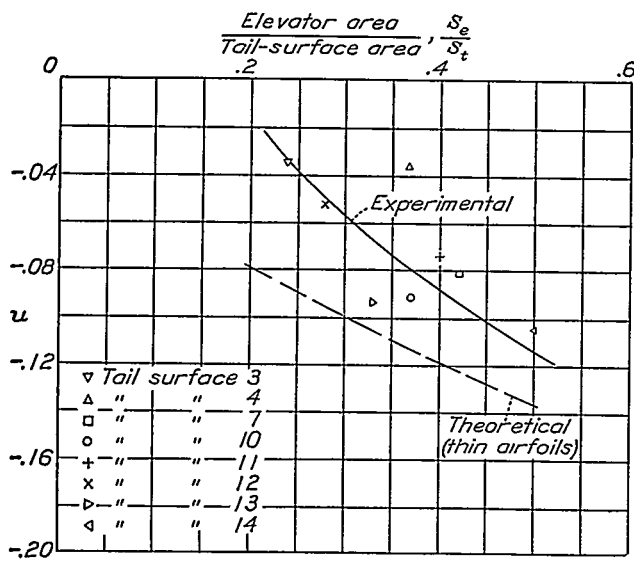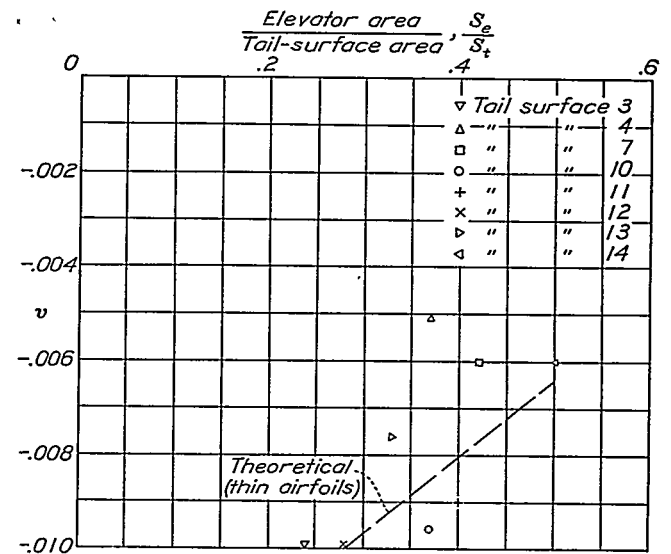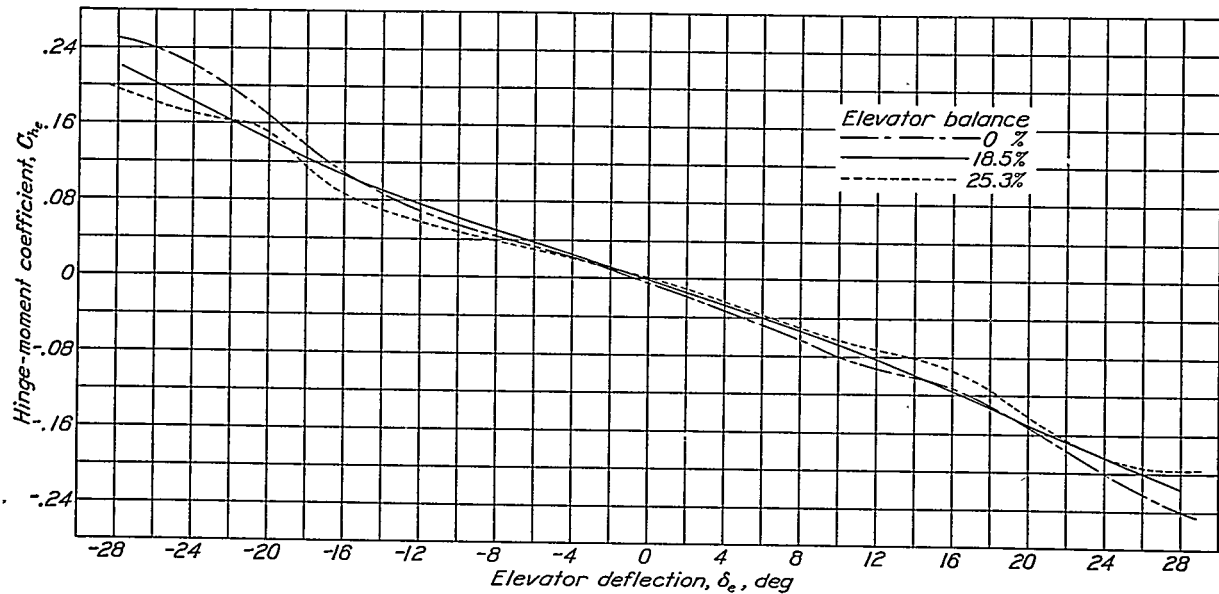
FIGURE 46.—Elevator hinge-moment coefficient against elevator deflection at various angles of attack for tail surface 17.

FIGURE 47.—Comparison of the theoretical and the experimental values of the parameter u.

$$u = \left(\frac{\partial C_{h_e}}{\partial C_N}\right)_{\delta_e}$$

FIGURE 48.—Comparison of the theoretical and the experimental values of the parameter v.

$$v = \left(\frac{\partial C_{h_e}}{\partial \delta_e}\right)_{\alpha_t} - u\left(\frac{\partial C_N}{\partial \delta_e}\right)_{\alpha_t}$$

FIGURE 49.—Elevator hinge-moment coefficient against elevator deflection at $\alpha_t = 0°$ for tail surfaces 4, 5, and 6.

FIGURE 50.—Drag coefficient against angle of attack at various elevator deflections for tail surface 1.

FIGURE 51.—Drag coefficient against angle of attack at various elevator deflections for tail surface 4.
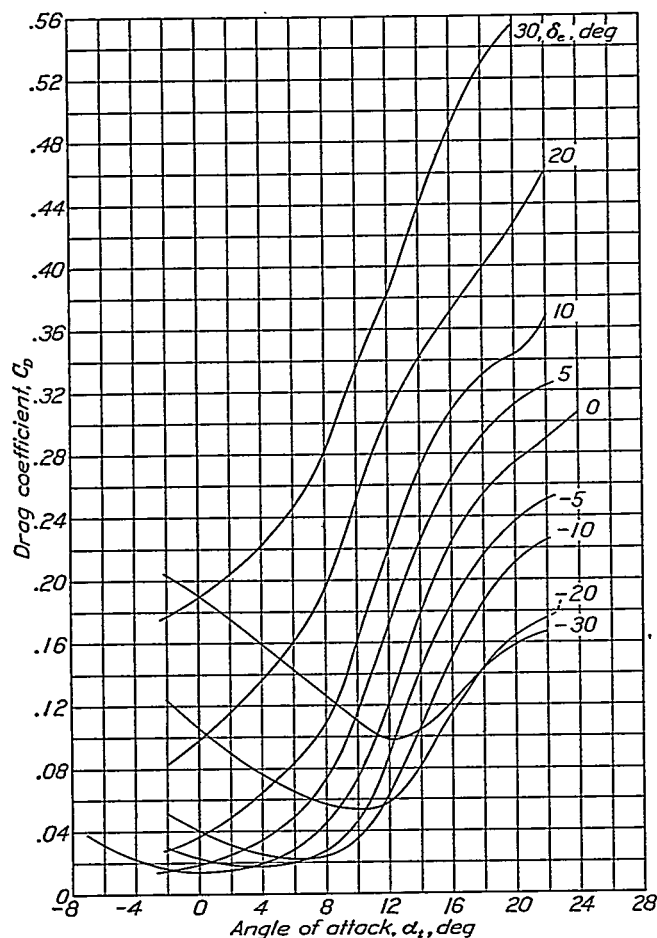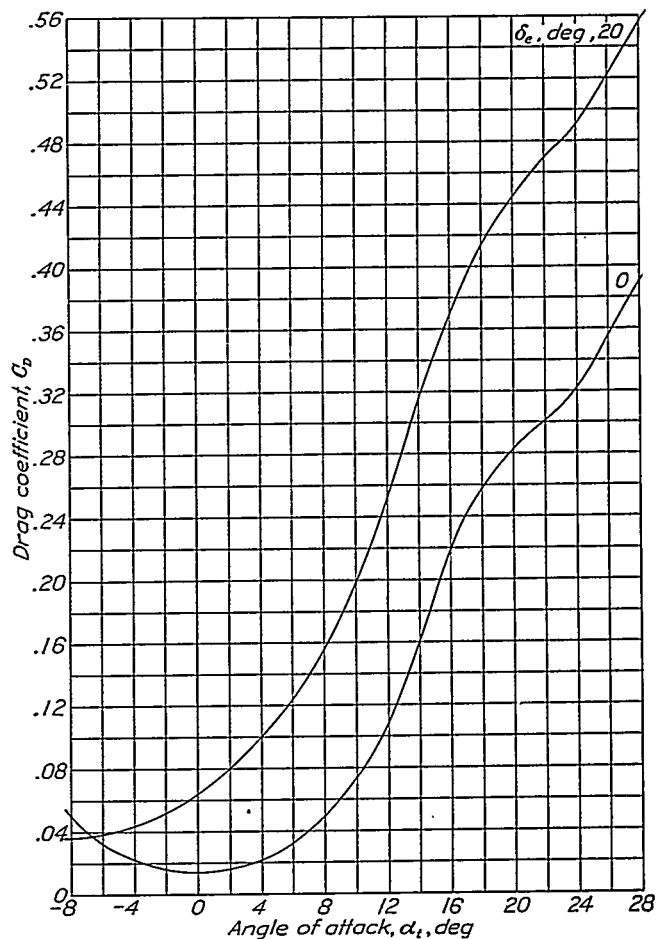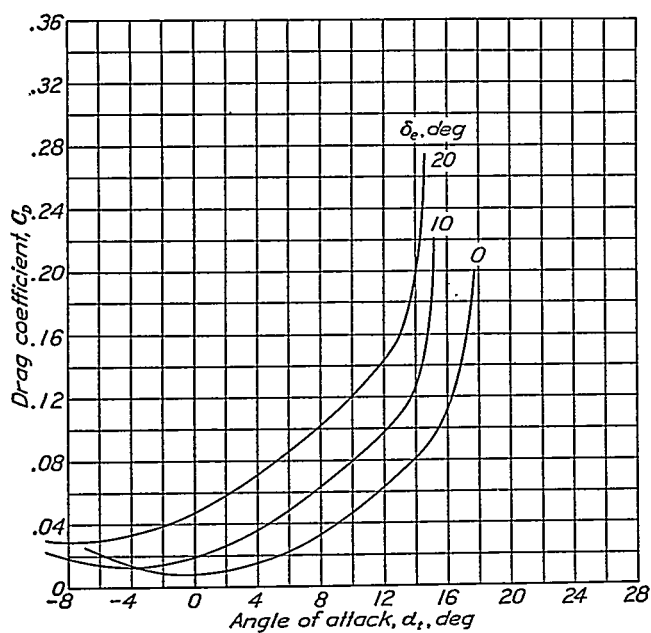

FIGURE 52.—Drag coefficient against angle of attack at various elevator deflections for tail surface 15.
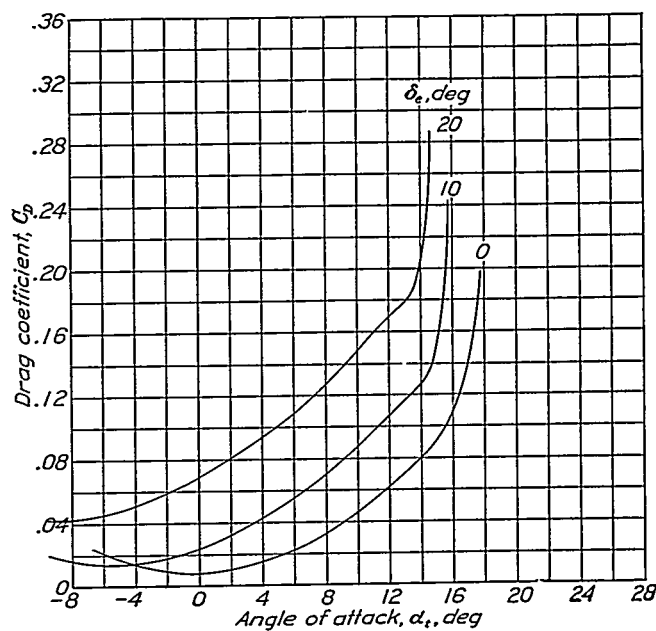

FIGURE 53.—Drag coefficient against angle of attack at various elevator deflections for tail surface 16.
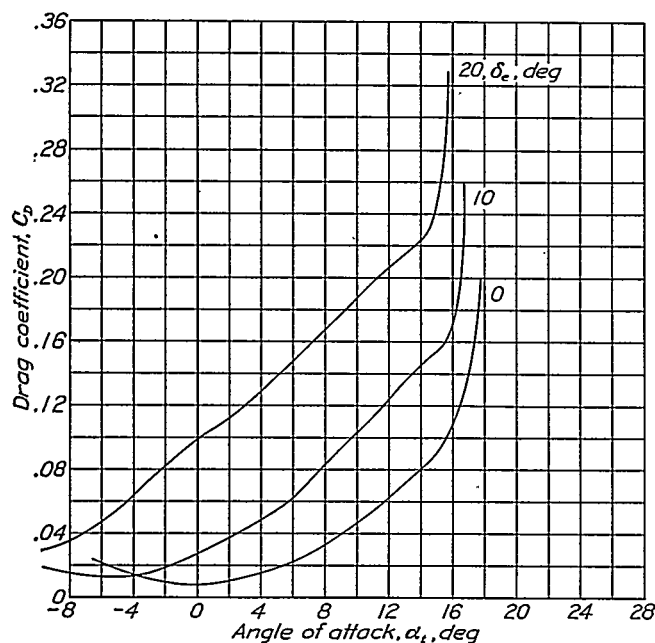
FIGURE 54.—Drag coefficient against angle of attack at various elevator deflections for tail surface 17.

CONCLUSIONS

1. The lifting-line theory predicts values of the slope of the curve of the normal-force coefficient about 10 percent higher than the experimental ones obtained for tail surfaces with aspect ratios from 3.5 to 4.

2. Experimental results of the effect of end plates are in good agreement with theory.

3. Thin-airfoil theory predicts values of the elevator effectiveness and the hinge moments that are somewhat larger than the experimental values.

LANGLEY MEMORIAL AERONAUTICAL LABORATORY,
NATIONAL ADVISORY COMMITTEE FOR AERONAUTICS,
LANGLEY FIELD, VA., *December 20, 1938.*

REFERENCES

1. Gorskii, V. P.: Aerodynamic Investigations of Tail Surfaces with Balanced and Unbalanced Elevators. Report No. 49, Central Aero-Hydrodynamical Inst. (Moscow) 1930, pp. 49–90.

2. Fuchs, Zygmunt: Wind-Tunnel Tests of Horizontal Tail Surfaces. Lwowskie Czasopismo Lotnicze (Lwow); Part I—vol. 1, no. 3, 1933, pp. 27–32; Part II—vol. 1, no. 4, 1933, pp. 41–53; Part III—vol. 2, no. 2, 1934, pp. 56–61; Part IV—vol. 3, no. 1, 1935, pp. 13–22.

3. Seiferth, R.: Experiments with Three Horizontal Empennages. T. M. No. 419, N. A. C. A., 1927.

4. Glauert, H.: Theoretical Relationships for an Aerofoil with Hinged Flap. R. & M. No. 1095, British A. R. C., 1927.

5. Blenk, Hermann: Der Eindecker als tragende Wirbelfläche. Z. f. a. M. M., Bd. V, Heft 1, Feb. 1925, S. 36–47.

6. Zimmerman, C. H.: Characteristics of Clark Y Airfoils of Small Aspect Ratios. T. R. No. 431, N. A. C. A., 1932.

7. Okamoto, Tetusi: Lift Coefficients of Wings with Various Cut-Outs. Jour. Aero. Res. Inst., Tokyo Imperial Univ., No. 105, May 1933, pp. 242–255 (Japanese text).

8. Wenzinger, Carl J.: Wind-Tunnel Investigation of Ordinary and Split Flaps on Airfoils of Different Profile. T. R. No. 554, N. A. C. A., 1936.

9. Hübner, Walter: The Effect of a Gap between Elevator and Stabilizer on the Static Stability and Maneuverability about the Lateral Axis in Flight. T. M. No. 701, N. A. C. A., 1933.

10. von Kármán, Th., and Burgers, J. M.: Single Wing with Shields at Ends. Vol. II, div. E, sec. 19 of Aerodynamic Theory, W. F. Durand, ed., Julius Springer (Berlin), 1935, pp. 211–212.

11. Jacobs, Eastman N., Pinkerton, Robert M., and Greenberg, Harry: Tests of Related Forward-Camber Airfoils in the Variable-Density Wind Tunnel. T. R. No. 610, N. A. C. A., 1937.